Mono(η^5-cyclopentadienyl)metal(II) Complexes with Thienyl Acetylide Chromophores: Synthesis, Electrochemical Studies, and First Hyperpolarizabilities

Tiago J. L. Silva,[†] Paulo J. Mendes,*[,‡] Ana M. Santos,[†] M. Helena Garcia,[†] M. Paula Robalo,[§,‖]
J. P. Prates Ramalho,[‡] A. J. Palace Carvalho,[‡] Marina Büchert,[⊥] Christian Wittenburg,[⊥] and Jürgen Heck[⊥]

[†]Centro de Ciências Moleculares e Materiais, Faculdade de Ciências, Universidade de Lisboa, Ed. C8, Campo Grande, 1749-016 Lisboa, Portugal

[‡]Centro de Química de Évora, Departamento de Química, Escola de Ciências e Tecnologia, Universidade de Évora, Rua Romão Ramalho 59, 7002-554 Évora, Portugal

[§]Centro de Química Estrutural, Instituto Superior Técnico, Universidade Técnica de Lisboa, Av. Rovisco Pais, 1049-001 Lisboa, Portugal

[‖]Área Departamental de Engenharia Química, Instituto Superior de Engenharia de Lisboa, Rua Conselheiro Emídio Navarro, 1, 1959-007 Lisboa, Portugal

[⊥]Institut für Anorganische und Angewandte Chemie, Universität Hamburg, Martin-Luther-King-Platz 6, D-20146 Hamburg

S *Supporting Information*

ABSTRACT: A series of mono(η^5-cyclopentadienyl)metal-(II) complexes with nitro-substituted thienyl acetylide ligands of general formula $[M(\eta^5\text{-}C_5H_5)(L)(C{\equiv}C\{C_4H_2S\}_nNO_2)]$ (M = Fe, L = κ^2-DPPE, n = 1, 2; M = Ru, L= κ^2-DPPE, 2 PPh$_3$, n = 1, 2; M = Ni, L = PPh$_3$, n = 1, 2) has been synthesized and fully characterized by NMR, FT-IR, and UV−Vis spectroscopy. The electrochemical behavior of the complexes was explored by cyclic voltammetry. Quadratic hyperpolarizabilities (β) of the complexes have been determined by hyper-Rayleigh scattering (HRS) measurements at 1500 nm. The effect of donor abilities of different organometallic fragments on the quadratic hyperpolarizabilities was studied and correlated with spectroscopic and electrochemical data. Density functional theory (DFT) and time-dependent DFT (TDDFT) calculations were employed to get a better understanding of the second-order nonlinear optical properties in these complexes. In this series, the complexity of the push−pull systems is revealed; even so, several trends in the second-order hyperpolarizability can still be recognized. In particular, the overall data seem to indicate that the existence of other electronic transitions in addition to the main MLCT clearly controls the effectiveness of the organometallic donor ability on the second-order NLO properties of these push−pull systems.

M = Fe, Ru or Ni; 1 or 2 thienyl rings; R=Ph; R'=Ph, -CH$_2$-
β_{corr}^{1500} = 80-224 x 10^{-30}esu
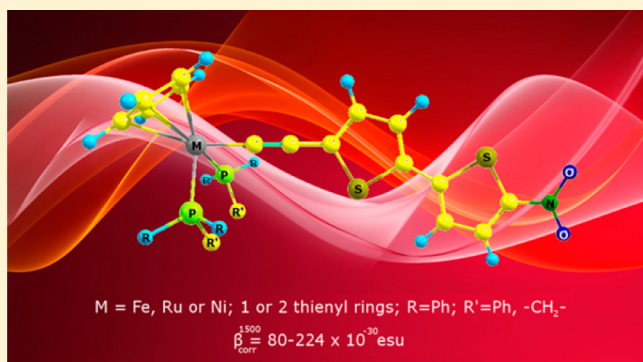
INTRODUCTION

Organometallic compounds have given rise to a great deal of interest owing to their application in the field of nonlinear optics (NLO).[1−11] Organometallic complexes (and organic molecules) have been shown as potential alternatives to the traditional inorganics due to fast and large NLO response, high optical damage thresholds, and structural diversity. In comparison to organic chromophores, organometallics can offer additional flexibility due to the presence of metal−ligand charge transfer excitations, usually at low energy and of high intensity, which are tunable due to the diversity of metal centers, oxidation states, ligand environments, and coordination geometries.

In order to obtain high second-order responses (molecular quadratic hyperpolarizability, β), strongly asymmetric systems

are needed. These systems can be obtained by combining a π-conjugated chain with electron donor and/or acceptor groups (D-π-A) in which metal centers can behave either as acceptor or donor groups by simply varying the metal and/or its oxidation state. During the last two decades, it has been found that high β values could be found for molecules in which the metal center is coplanar with the π-conjugated chain. Concerning this feature, systematic studies were made by our group and others on mono(η^5-cyclopentadienyl)metal and pseudo-octahedral complexes with benzene- or thiophene-

Scheme 1. Synthesis and Atom Labeling of the Fe(II), Ru(II), and Ni(II) Complexes
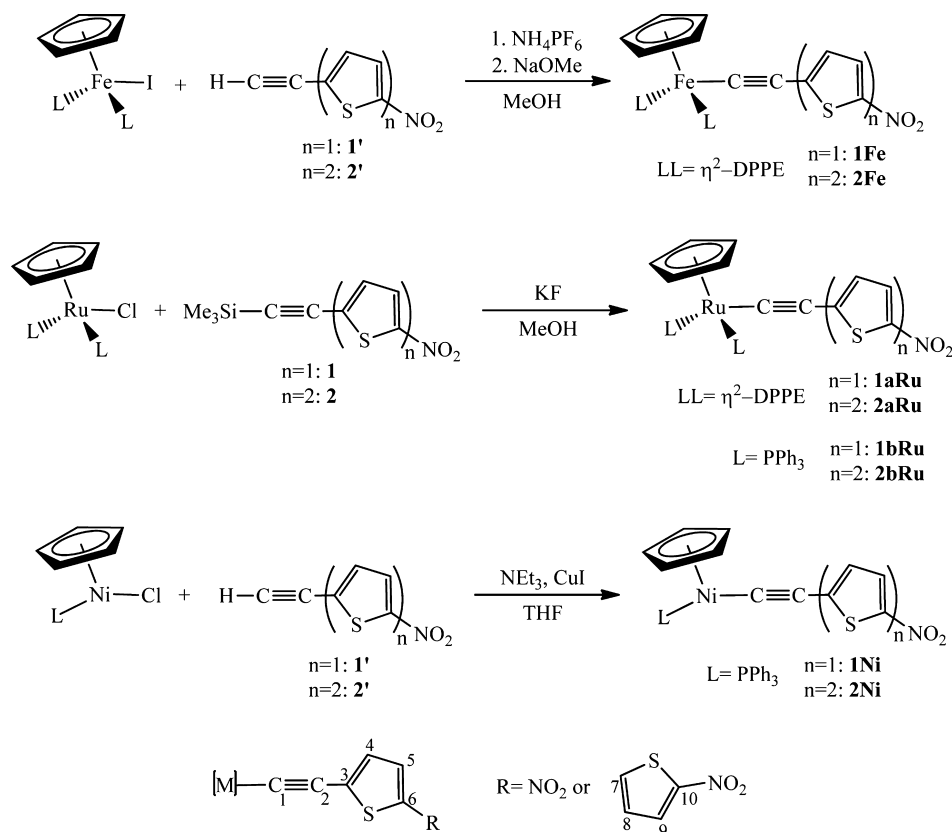
based conjugated chains, coordinated to the metal centers through nitrile or acetylide linkages.[7,12−23]

In many cases, the structure−NLO activity trends were revealed to be similar to those observed in organic compounds: i.e., nonlinearities can be enhanced by either increasing the conjugation length and ease of the electronic delocalization of the hyperpolarizable chromophore or increasing the strength of donor or acceptor groups. For example, very efficient NLO responses were found when strong electron donors such as readily oxidizable 18-electron iron(II) and ruthenium(II) organometallic moieties were coupled with strong electron acceptors such as a nitro group.[5,7,21,23] In addition, compounds derived from metal half-sandwich moieties possessing benzenoid acetylide ligands revealed better NLO properties than the nitrile analogues, probably due to more favorable metal−ligand coupling through enhanced metal to ligand π back-bonding.[4,20,24,25]

However, some aspects of the relationship between structural features and NLO activity in these systems remain unclear. Replacing phenyl rings with heterocycles improves the ease of delocalization, thus yielding a good basis for high second-order NLO responses, as already proven in organic chromophores[26−28] and in a series of mono(η^5-cyclopentadienyl)-ruthenium(II) thiophene acetylide[22] and mono(η^5-cyclopentadienyl)iron(II) thiophene nitrile[16] complexes. However, the effect on the optical nonlinearities was found to be not easily understandable. For instance, quadratic nonlinearities on metal acetylides were found to be[7] (i) not consistently increased on replacment of phenyl by a pyridyl ring, (ii) decreased on incorporation of a furanyl ring, and (iii) almost independent of the relative location of the thienyl and phenyl rings in two-ring acetylide ligands. The effect of increasing the

conjugation length of the chromophores also showed contradictory results. For benzene-based acetylides an increase in β_{corr} value was found (β_{corr} taking into account the dispersion effects using a two-level model, TLM[29]) upon an increase in chain length, in spite of some saturation of the β_{corr} signal for long chains.[7,13] In the case of benzene-based nitrile metal complexes, an attempt to increase the observed intrinsic quadratic hyperpolarizability by replacing a phenyl with a biphenyl unit was unsuccessful due to the significant torsion angle in the latter ligand, which leads to the conjugation breaking.[21,17] The higher quadratic hyperpolarizability obtained when the conjugation length is increased without affecting planarity by insertion of a vinylene unit further supported this assumption. In the case of metal complexes presenting oligo-thiophene chromophores, our studies on mono(η^5-cyclopentadienyl)iron-(II) nitrile compounds showed some constancy of β_{corr} values upon chain lengthening due to a compromise between the conjugation length and the metal to ligand charge transfer.[16] In addition, β values do not increase regularly upon chain lengthening on (porphinato)zinc(II) thiophene acetylides.[30] The effect of different coligands on quadratic hyperpolariz-abilities has been also studied. In fact, different coligands can modify donor strength of the organometallic moieties. For example, replacing two CO ligands by DPPE results in a significant increase in the quadratic hyperpolarizability of mono(η^5-cyclopentadienyl)iron(II) benzene acetylides,[7] while subtle variations in the hyperpolarizability are observed on replacing DPPE by (+)-DIOP in related mono(η^5-cyclopentadienyl)iron(II) nitriles[17] or on replacing DPPE by DPPM or two PPh3 ligands in pseudo-octahedral acetylide complexes.[7] However, when TLM is taken into account, the effect of replacing DPPE ($\beta_{\text{corr}} = 161 \times 10^{-30}$ esu) by two PPh3

($\beta_{corr} = 96 \times 10^{-30}$ esu) or PMe$_3$ ($\beta_{corr} = 38 \times 10^{-30}$ esu) on the quadratic hyperpolarizability of mono(η^5-cyclopentadienyl)-ruthenium(II) acetylides cannot be underestimated.[7]

The effect of metal variation on quadratic hyperpolarizabilities needs also some attention. For mono(η^5-cyclopentadienyl)metal complexes, for example, studies suggest a trend on quadratic nonlinearity as $\beta(\text{Ni}) < \beta(\text{Fe}) \leq \beta(\text{Ru})$ for benzene acetylides having one aryl ring.[20,31−33] When the dispersion effects are taken into account using the TLM, the corresponding corrected β values for ruthenium complexes were revealed clearly to be larger than those found for iron and Ni complexes: $\beta_{corr}(\text{Ni}) \leq \beta_{corr}(\text{Fe}) < \beta_{corr}(\text{Ru})$.[7] For the corresponding nitrile derivatives, however, both β and β_{corr} values for iron are clearly higher than those found for ruthenium and nickel complexes, thus leading to Ni < Ru < Fe.[21] For the compounds presenting two benzene rings in the conjugated system, the limited data available for direct comparison seem to indicate that both β and β_{corr} follow the same trend (Ni < Ru < Fe),[7,21] but further studies will be necessary to confirm these results.

In our continuing effort to establish detailed structure−NLO activity correlations and to complement the previously reported studies on mono(η^5-cyclopentadienyl)metal(II) complexes presenting benzene- or thiophene-based conjugated chromophores, it seems that it is of importance to further study the quadratic hyperpolarizability of these systems incorporating acetylide thiophene chromophores. Our goal is to contribute to the clarification of the aforementioned issues with particular relevance for the role of different organometallic donor moieties, on the quadratic hyperpolarizabilities. Thus, we report herein the syntheses of a series of mono(η^5-cyclopentadienyl)metal(II) complexes with nitro-substituted thienyl acetylide ligands of general formula [M(η^5-C$_5$H$_5$)(L)-(C≡C{C$_4$H$_2$S}$_n$NO$_2$)] (M = Fe, L = κ^2-DPPE, n= 1, 2; M = Ru, L = κ^2-DPPE, 2 PPh$_3$, n = 1, 2; M = Ni, L = PPh$_3$, n = 1, 2). Spectroscopic and electrochemical data and theoretical calculations on model complexes using DFT and TDDFT are used to explain the experimental quadratic hyperpolarizabilities of these compounds. Measurements of these properties were carried out by HRS at the fundamental wavelength of 1500 nm to avoid superposition of the UV−vis absorptions and the second harmonic signal to ensure more reliable analysis of the results on the basis of the well-known two-level model.

■ RESULTS AND DISCUSSION

Synthesis and Spectroscopic Studies. Trimethyl((5-nitrothiophen-2-yl)ethynyl)silane (**1**) and trimethyl((5′-nitro-2,2′-bithiophen-5-yl)ethynyl)silane (**2**) ligands were obtained in good yields by Sonogashira cross-coupling of ethynyltrimethylsilane with the corresponding nitro-thiophene bromides. Subsequent removal of the trimethylsilyl protecting group with base afforded 2-ethynyl-5-nitrothiophene (**1′**) and 5-ethynyl-5′-nitro-2,2′-bithiophene (**2′**).

The acetylide complexes were prepared in good yields (54−80%) using the synthetic methodologies successfully utilized for the preparation of iron(II),[20] ruthenium(II),[34] and nickel(II)[33] σ-arylacetylides (Scheme 1). Reaction of [Fe(η^5-C$_5$H$_5$)-(DPPE)I] with **1′** and **2′** in refluxing methanol, in the presence of NH$_4$PF$_6$, afforded iron vinylidene complexes, which were deprotonated in situ using sodium methoxide to give the σ-acetylide products. The vinylidene route has been widely used in the preparation of ruthenium alkynyls with NLO properties.[7] However, we adopted the method of Xia and Selegue,[34] in

which the deprotection of the trimethylsilyl alkynes **1** and **2** with KF in methanol in the presence of the organo-ruthenium chloride gave the ruthenium alkynyls in a single step. Finally, the nickel derivatives were obtained by transmetalation reactions catalyzed by copper(I) iodide of the suitable terminal alkyne **1′** or **2′** with [Ni(η^5-C$_5$H$_5$)(PPh$_3$)Cl], in the presence of triethylamine. The compounds are fairly stable toward oxidation in air and to moisture both in the solid state and in solution and were characterized by IR and ^{1}H, ^{13}C, and ^{31}P NMR spectroscopy and satisfactory microanalyses.

For all compounds, a characteristic $\nu(\text{C}\equiv\text{C})$ band in the IR spectrum was found in the range 2005−2074 cm^{-1}. A significant low-energy shift was observed in this band upon coordination of the ethynyl ligands, in particular for iron and ruthenium complexes (Table 1). The negative shifts have been related to enhanced π back-donation from the metal d orbitals to the π^* orbital of the C≡C group, which leads to a decrease in the C≡C bond order. It is well accepted that π back-bonding has a synergic effect with the dominant σ bond with the reinforcement of the binding. This π-back-bonding effect was found to be relatively small in comparison to the M−C σ bond by theoretical calculations on similar mono(η^5-cyclopentadienyl)-derived molecules[35] and should be also the case in the compounds studied in this work. In the present study, the observed negative shifts show the expected trend, considering the π-donor ability of the organometallic fragment ([Fe] > [Ru] ≫ [Ni]). In addition, the thiophene chain lengthening leads to a less effective π back-donation interaction and no significant differences are observed for Ru complexes by the presence of different phosphane coligands. The magnitude of the π back-donation interaction is higher for the compounds studied in this work in comparison to related thiophene nitrile[16,15] and benzene acetylide[4,7,20,25,33,36] complexes.

^{1}H and ^{13}C NMR resonances for the cyclopentadienyl ring are in the range usually observed for neutral iron(II),[20,32,37] ruthenium(II),[22,25,32] and nickel(II)[33,38,39] complexes and are relatively insensitive to the chain lengthening of the acetylide ligand. Considering the thiophene ligand protons, an overall shielding effect upon coordination was observed, especially for the H4 protons (see Scheme 1 for numbering), indicating an electronic flow toward the aromatic ligand due to π back-donation involving the metal center. The shifts in the resonances are consistent with the possibility of some contribution of an allenylidene form in solution. ^{13}C NMR data show an expected deshielding on the C≡C carbons (C1 and C2) upon coordination, whereas for the ring carbons more significant changes were observed for those in the ring adjacent to the acetylide group, in agreement with the trends observed in the ^{1}H NMR spectra. ^{31}P resonances for the phosphane coligands are in the range usually observed for mono(η^5-cyclopentadienyl)iron(II), -ruthenium(II) and -nickel(II) complexes and are relatively insensitive to the chain lengthening of the acetylide ligand.

The optical absorption spectra of all complexes were recorded using 1.0×10^{-5} M solutions in chloroform. The spectrum for **2aRu** typifies the behavior of the compounds studied in this work (Figure 1), and the optical data are summarized in Table 2. The main feature of these spectra is the presence of an intense band in the range 484−613 nm and bands at higher energy (with peak positions in the range 286−410 nm), depending on the organometallic fragment and thiophene chromophore. The band at lower energy has been attributed, in parent benzene compounds, to a MLCT (metal to

Table 1. Selected IR and ^{1}H and ^{13}C NMR Data^a

| compd | ν(C≡C) /cm^{-1} | ^{1}H (δ/ppm) | | ^{13}C (δ/ppm) | | | | | |
		H4	H5	C1	C2	C3	C4	C5	C6
1Fe^b	2005 (−96)	5.92 (−1.49)	7.60 (−0.40)	141.90 (54.45)	118.52 (43.39)	140.05 (11.26)	125.37 (−7.67)	131.67 (2.59)	143.34 (−4.41)
2Fe^b	2024 (−72)	6.00 (−1.44)	7.17 (−0.39)	142.28 (55.98)	115.24 (38.70)	135.42 (12.39)	126.73 (2.63)	128.42 (−7.15)	127.45 (−9.47)
1aRu	2023 (−78)	5.81 (−1.36)	7.53 (−0.27)	143.36 (57.32)	108.76 (33.63)	140.51 (11.36)	125.47 (−6.69)	130.76 (2.64)	142.43 (−8.86)
1bRu	2019 (−82)	6.39 (−0.78)	7.78 (−0.02)	133.10 (47.06)	111.83 (36.70)	143.00 (13.85)	125.38 (−6.78)	131.04 (2.92)	142.39 (−8.90)
2aRu	2037 (−59)	5.63 (−1.58)	7.00 (−0.23)	145.25 (61.16)	127.55 (51.57)	141.76 (17.43)	119.66 (−6.43)	126.90 (−7.30)	125.82 (−10.34)
2bRu	2037 (−59)	6.53 (−0.68)	7.19 (−0.04)	140.21 (56.12)	108.43 (32.45)	146.80 (22.47)	126.70 (0.61)	127.92 (−6.28)	137.94 (1.78)
1Ni	2074 (−27)	6.17 (−1.00)	7.53 (−0.27)	115.24 (29.20)	111.35 (36.22)	137.65 (8.50)	126.92 (−5.24)	129.36 (1.24)	145.30 (−5.99)
2Ni	2074 (−22)	6.27 (−0.94)	6.94 (−0.29)	134.46 (50.37)	110.79 (34.81)	132.11 (7.78)	128.98 (2.89)	126.26 (−7.94)	130.36 (−5.80)

^{a}Differences on IR ν(C≡C) ($\nu_{complex} - \nu_{ligand}$) and NMR ^{1}H and ^{13}C resonances of thiophene ligands ($\delta_{complex} - \delta_{ligand}$) upon coordination to the organometallic fragments are shown in parentheses (ligand **1′** or **2′**). NMR data are given in CDCl$_3$ except where otherwise indicated. ^{b}NMR data in d-acetone.
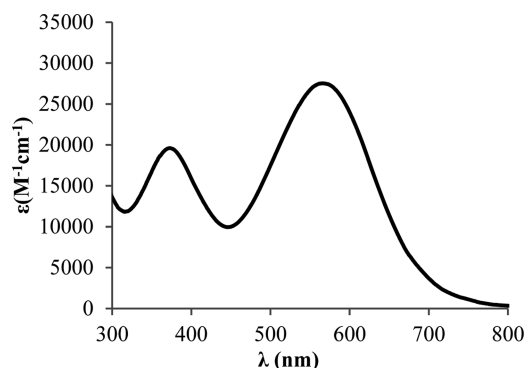

Figure 1. UV−visible spectrum for **2aRu** in chloroform.

Table 2. Optical Spectral Data for Fe, Ru, and Ni Complexes in Chloroform Solution (ca. 1.0×10^{-5} mol dm^{-3})

compd	λ/nm (ε/10^4 M^{-1} cm^{-1})
1Fe	578 (1.3), 363 (0.7)
2Fe	613 (1.5), 400 (1.1)
1aRu	517 (2.0), ∼320 (sh)
1bRu	536 (2.2), ∼310 (sh)
2aRu	566 (2.8), 373 (2.0)
2bRu	580 (2.4), 374 (1.2)
1Ni	484 (0.7),^{a} 404 (0.2),^{a} 286 (0.9)
2Ni	506 (2.3), 410 (sh), 350 (sh)

^{a}Obtained from a fit with multiple Gaussian bands.

ligand charge transfer) transition, whereas the high-energy bands are ascribed to internal transitions occurring at the acetylide chromophores and or/organometallic moiety.[20,24,25,36]

In fact, according to the results of our TDDFT calculations (see below) the lower energy bands, which are the key for second-order nonlinear optical properties, can be attributed to MLCT. The energy and intensity of these bands depend mainly on the metal and acetylide chromophore chain length and, to a lesser extent, on the different phosphane coligands in the Ru complexes. The energy of these bands follows the expected trend, considering the differences on the electronic properties of the metal (Ni > Ru > Fe). These energies are lower than those found in already reported benzene-based iron(II),[20] ruthenium(II)[24,25] and nickel(II)[33] acetylide analogues and related iron(II)[16] and ruthenium(II)[15] nitrile compounds and are within the range of those observed in a series of ruthenium acetylides with an end-capping nitro group and thienyl and benzene entities in the conjugation chain.[22] The chain lengthening of the chromophore led to a bathochromic effect on these bands for all complexes. This effect is opposite of that already reported for benzene-based iron(II),[20] ruthenium-(II)[24,25] and nickel(II)[33] acetylide analogues and also for related iron(II)[16] and ruthenium(II)[15] nitrile compounds. This can be explained by an improved planarity that can be expected from: (i) the limited steric hindrance of dithienyl in comparison to the biphenyl moiety and (ii) the higher level of electronic coupling between the organometallic fragment and the thiophene chromophores through an acetylide linkage in comparison to a nitrile bond. Considering point ii, IR data revealed that the magnitude of π back-donation interaction is stronger for the compounds studied in this work, thus favoring a more effective conjugation and improved planarity in comparison to the related thiophene nitrile and benzene-based acetylide complexes (see above).

UV/vis absorption spectra were also recorded for all complexes in other solvents with different polarities (ethyl ether and DMF), in the wavelength range 200−800 nm, to examine the solvatochromic behavior of the lowest-energy band (Table 3). The results showed a bathochromic shift for all

Table 3. Solvatochromic Behavior of the Lowest-Energy Bands of All Complexes

	λ/nm			
compd	Et$_2$O	CHCl$_3$	DMF	$\Delta\lambda$ ($\Delta\bar{\nu}/10^3$ cm^{-1})
1Fe	524	578	601	77 (2.4)
2Fe	582	613	631	49 (1.3)
1aRu	484	517	538	54 (2.1)
1bRu	498	536	538	40 (1.5)
2aRu	534	566	577	43 (1.4)
2bRu	554	580	585	31 (1.0)
1Ni	468	484	501	33 (1.4)
2Ni	494	506	510	16 (0.6)

complexes upon increasing solvent polarity. This positive solvatochromic behavior is characteristic of transitions with an increase of the dipole moment upon photoexcitation. The magnitude of this red shift depends on the organometallic fragment ([Fe] > [Ru] > [Ni]; DPPE > 2 PPh$_3$) and chain lengthening of the coordinated acetylide ligand ([M]-C≡C{C$_4$H$_2$S}$_n$NO$_2$: $n = 1 > n = 2$). The absolute values of the solvatochromic shift are almost comparable to those found for benzene-based acetylide ruthenium(II)[24,25] (35−39 nm) analogues but are large in comparison to those for benzene-based iron(II)[20] (13−23 nm) acetylide analogues and also for related iron(II)[16] (23−32 nm) and ruthenium(II)[15] (14−30 nm) nitrile compounds.

DFT Calculations. Recently, DFT calculations on a series of mono(η^5-cyclopentadienyl)iron(II) and -ruthenium(II) thiophene acetylide complexes with general formula M(η^5-C$_5$H$_5$)-(H$_2$PCH$_2$CH$_2$PH$_2$)(C≡C{C$_4$H$_2$S}Y) (Y = donor and acceptor groups) have been carried out by our group in order to study structure−static quadratic hyperpolarizability relationships.[23,40] The results have shown that the traditional qualitative arguments for enhancing second-order nonlinear optical responses were applicable to these complexes, thus leading to the prediction of higher hyperpolarizabilities for M(η^5-C$_5$H$_5$)-(H$_2$PCH$_2$CH$_2$PH$_2$)(C≡C{C$_4$H$_2$S}NO$_2$) (M = Fe, Ru), in which the strong electron donor organometallic fragment was combined with the better acceptor group NO$_2$. In this work we extend the DFT study to nickel complexes and to compounds with two thienyl rings. In addition, the effect of different phosphane coligands in the Ru complexes was evaluated. As a compromise between accuracy and computational effort, three simplifications were used in the calculations: (i) only the first 24 lower excitation states were computed in TDDFT studies, (ii) dephenylated phosphanes were used, i.e., H$_2$PCH$_2$CH$_2$PH$_2$ instead of DPPE and PH$_3$ instead of PPh$_3$, and (iii) isolated molecules in the gas phase were used (i.e., no solvent corrections were employed). The adequacy of the simplification (i) was checked by the use of a larger number of excited states for simulating the electronic spectra of **1a′Ru**, and the results were compared to those obtained with 24 excited states. The adequacy of the simplifications (ii) and (iii) was checked by a comparison between the calculated optical data obtained for the model complexes **1a′Ru** and **2a′Ru** and real **1aRu** and **2aRu** with experimental data. All these results are included in

the Supporting Information (Figures S1−S5 and Tables S1−S2). The computed data showed that the use of phenylated phosphanes and solvated media does not result in a significantly better match between the calculated and experimental data. In addition, no differences in the simulated electronic spectra for the lowest energy bands, which are the important ones for NLO, were achieved by the use of a larger number of excitation states in TDDFT studies. Thus, the use of these approximations gives a good description of the experimental results with significant gain in computational effort.

Figure 2 shows the structure and atom labeling of the model complexes used in calculations, and Table 4 gives selected
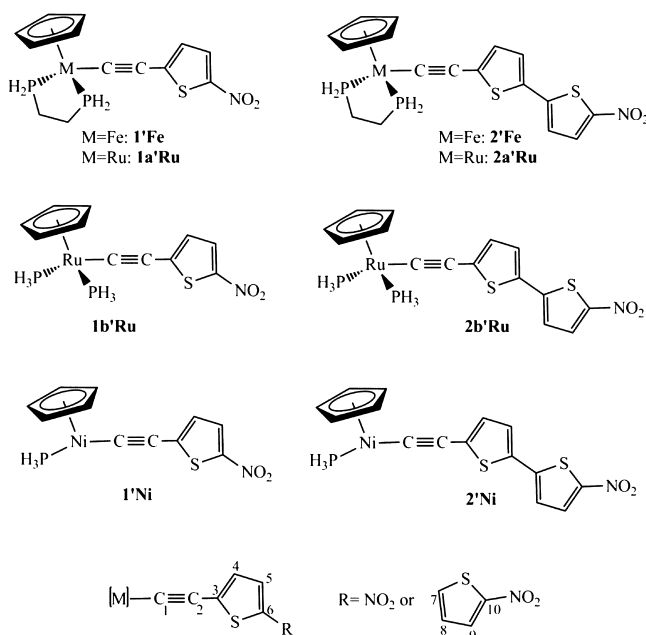

Figure 2. Structure and atom labeling of the model complexes used in DFT calculations.

structural data for the optimized structures in the gas phase. The optimized structures for all complexes are shown in the Supporting Information (Figures S6−S13).

The calculated angles and bond lengths are consistent with experimental crystal data for related mono(η^5-cyclopentadienyl)metal σ-arylacetylides. For instance, the calculated M−Cp, M−C1, and C1−C2 bond lengths and M−C1−C2 and P−M−C1 bond angles are within or close to the range of experimental reported values for iron (Fe−Cp, 2.060−2.122 Å; Fe−C1, 1.856−1.910 Å; C1−C2, 1.202−1.236 Å; Fe−C1−C2, 177.0−178.7°; P−Fe−C1, 85.1−85.5°),[20,37] ruthenium (Ru−Cp, 2.222−2.260 Å; Ru−C1, 1.974−2.017 Å; C1−C2, 1.214−1.232 Å; Ru−C1−C2, 173.7−178.0°; P−Ru−C1, 85.9−90.8°),[22,24,25,36] and nickel (Ni−Cp, 2.063−2.146 Å; Ni−C1, 1.840−1.856 Å; C1−C2, 1.191−1.209 Å; Ni−C1−C2, 173.9−177.7°)[36] complexes. The calculations predict a decrease of the C1−C2 bond order and a decrease of the C2−C3 bond length of the acetylide ligands upon coordination, which is consistent with a metal to ligand π back-donation interaction that was observed experimentally (see above). It is interesting to note that, in spite of some overestimation of ν(C≡C), DFT calculations predict the experimental trend on the magnitude of the metal to ligand π-back-donation interaction when they consider the effect of different metal and chain lengthening of the acetylide chromophores. The concept of bond length

Table 4. Selected Calculated Structural Data for the Fe, Ru, and Ni Model Complexes

| compd	1'Fe[a]	2'Fe	1a'Ru[b]	1b'Ru	2a'Ru	2b'Ru	1'Ni	2'Ni
				Bond Lengths (Å)[c]				
M–Cp[d]	2.128	2.128	2.264	2.258	2.263	2.257	2.154	2.154
M–P[e]	2.297	2.295	2.391	2.400	2.391	2.400	2.260	2.258
M–C1	1.898	1.901	1.998	2.001	2.001	2.004	1.853	1.854
C1–C2	1.237 (1.211)	1.237 (1.212)	1.236 (1.211)	1.235 (1.211)	1.236 (1.212)	1.235 (1.212)	1.230 (1.211)	1.230 (1.212)
C2–C3	1.393 (1.406)	1.394 (1.405)	1.392 (1.406)	1.393 (1.406)	1.392 (1.405)	1.393 (1.405)	1.398 (1.406)	1.398 (1.405)
BLA	0.022 (0.037)	0.031 (0.042)	0.019 (0.037)	0.021 (0.037)	0.029 (0.042)	0.030 (0.042)	0.027 (0.037)	0.035 (0.042)
				Bond Angles (deg)[c]				
M–C1–C2	179.3	179.2	179.6	179.2	179.9	178.6	178.2	178.6
C1–C2–C3	179.9 (179.4)	179.4 (179.5)	179.4 (179.4)	179.3 (179.4)	179.8 (179.5)	179.6 (179.5)	179.6 (179.4)	179.9 (179.5)
P–M–C1[f]	86.8	86.6	84.8	85.0	84.7	84.6	90.3	90.3
P1–M–P2	86.3	86.3	83.5	92.7	83.5	92.7		
P1–M–Cp[g]	129.1	129.2	131.2	127.7	131.2	127.9	137.1	137.3
C1–M–Cp	124.6	124.7	125.2	125.0	125.1	124.8	132.3	132.1
Dh[h]		−179.7 (−179.9)			179.9 (−179.9)	179.7 (−179.9)		−179.5 (−179.9)
				ν(C≡C) (cm^{-1})[i]				
	2072 (−67)	2071 (−63)	2074 (−65)	2081 (−58)	2072 (−62)	2078 (−56)	2116 (−23)	2114 (−20)

[a]Bond lengths and angles taken from ref 23. [b]Bond lengths and angles taken from ref 40. [c]Calculated bond lengths and angles of thiophene ligands HC≡C{C$_2$H$_4$S}$_n$-NO$_2$ are shown in parentheses. [d]Average M–C(Cp). [e]Average M–P1/P2 (M = Fe, Ru) bond lengths. [f]Average P1/P2–M–C1 (M = Fe, Ru) bond angles. [g]Average P1/P2–M–Cp (M = Fe, Ru) bond angles. [h]Dihedral angle (C5–C6–C7–C8). [i]Differences in calculated ν(C≡C) ($\nu_{complex} - \nu_{ligand}$) upon coordination to the organometallic fragments are shown in parentheses.

Table 5. Optical Data for 1′ and 2′ and the Studied Model Fe(II), Ru(II), and Ni(II) Complexes Obtained by Using TDDFT Calculations

compd	λ_{exp}[a] (nm)	λ_{eg}[b] (nm)	f[c]	attribution[d]	character of the CT[e]
1′	346	341	0.356	H → L (97)	C≡C (58), T1 (42) → NO$_2$ (100)
2′	410	429	0.648	H → L (99)	C≡C (33), T1 (67) → T2 (18), NO$_2$ (82)
	281	316	0.115	H-1 → L (37), H → L+1 (53)	C≡C (14), T1 (79), T2 (7) → NO$_2$ (100)
1′Fe[f]	578	468	0.390	H → L (75), H-1 → L+3 (10)	Fe (39), C≡C (25), T1 (30), Cp (6) → NO$_2$ (87), P (13)
	363	452	0.080	H-1 → L+3 (40), H-1 → L+2 (18), H → L (20)	Fe (57), Cp (3), C≡C (40) → NO$_2$ (27), P (67), T1 (6)
		321	0.106	H-3→L (92)	Fe (75), Cp (15), C≡C (10) → NO$_2$ (83), T1 (17)
2′Fe	613	559	0.710	H→L (98)	Fe (36), C≡C (37), Cp (5), T1 (20), P (2) → NO$_2$ (61), T2 (39)
	400	378	0.242	H-3 → L (33), H → L+1 (46)	Fe (47), C≡C (47), Cp (6) → NO$_2$ (58), T2 (26), P (16)
1a′Ru[g]	517	470	0.355	H → L (72), H → L+1 (24)	Ru (46), C≡C (54) → T1 (5), NO$_2$ (77), P (18)
	320	451	0.172	H → L (24), H → L+1 (67)	T1 (40), C≡C (60) → Cp (27), NO$_2$ (17), P (56)
		310	0.102	H-4 → L (21), H-3 → L (74)	Ru (56), P (2), T1 (23), Cp (19) → NO$_2$ (100)
1b′Ru	536	473	0.091	H → L (21), H → L+1 (71)	T1 (43), C≡C (57) → Ru (9), Cp (33), NO$_2$ (11), P (47)
	310	446	0.472	H → L (77), H → L+1 (20)	Ru (41), C≡C (59) → T1 (5), NO$_2$ (82), P (10), Cp (3)
		308	0.050	H-4 → L (72), H-3 → L (24)	Ru (16), T1 (80), Cp (4) → NO$_2$ (86), C≡C (12), P (2)
		304	0.060	H-4 → L (17), H-3 → L (19), H-3 → L+1 (17)	Ru (43), C≡C (6), T1 (48), Cp (3) → NO$_2$ (76), P (24)
2a′Ru	566	568	0.760	H → L (99)	Ru (32), Cp (7), C≡C (38), T1 (20), P (3) → T2 (39), NO$_2$ (61)
	373	380	0.158	H-3 → L (38), H → L+2 (30), H → L+3 (10)	Ru (54), Cp (8), C≡C (38) → T1 (3), T2 (26), NO$_2$ (55), P (16)
2b′Ru	580	552	0.773	H → L (99)	Ru (30), Cp (5), C≡C (39), T1 (24), P (2) → T2 (38), NO$_2$ (62)
	374	378	0.103	H-2 → L (75)	Ru (64), Cp (18), C≡C (13), P (5) → T1 (9), T2 (32), NO$_2$ (59)
		372	0.221	H-3 → L (49), H → L+2 (44)	Ru (53), Cp (12), C≡C (29), P (6) → T1 (14), T2 (31), NO$_2$ (55)
1′Ni	484	438	0.395	H → L (96)	Ni (34), Cp (41), C≡C (25) → T1 (26), NO$_2$ (74)
	404	350	0.183	H-1 → L (92)	Ni (37), P (2), Cp (50), C≡C (11) → T1 (25), NO$_2$ (75)
	286	252	0.160	H-12 → L+1 (10), H-7 → L+1 (42)	NO$_2$ (26), Cp (44), C≡C (30) → Ni (33), P (60), T1 (7)
2′Ni	506	521	0.273	H → L (36), H-1 → L+1 (20)	T1 (77), C≡C (23) → P (36), Cp (9), NO$_2$ (55)
	410	510	0.364	H-4 → L+1 (16), H → L (57)	Ni (24), Cp (3), C≡C (24), T1 (49) → P (15), T2 (24), NO$_2$ (61)
	350	410	0.141	H-1 → L (95)	Ni (38), P (1), Cp (57), C≡C (4) → T1 (8), T2 (39), NO$_2$ (53)
		351	0.172	H → L+2 (81)	Ni (26), Cp (28), C≡C (46) → T1 (16), T2 (24), NO$_2$ (60)

[a]Experimental data. [b]Absorption wavelength of the main transitions. [c]Oscillator strength. [d]Abbreviations: H, HOMO; L, LUMO. The percentage of the contribution is shown in parentheses. [e]Based on the represented molecule fragments (overall percentage of the charge transfer given in parentheses). Abbreviations: Cp, cyclopentadienyl; C≡C, acetylide group; T, thiophene rings (T1, close to C≡C; T2, close to NO$_2$); P, phosphane coligands. [f]Reference 23. [g]Reference 40.

alternation (BLA), defined as the difference between the average carbon−carbon adjacent bond lengths along a conjugated backbone, was found to be an important parameter that can be correlated with the optical nonlinearities of organic and organometallic/coordination complexes.[41−43] The calculated BLA parameter for the model complexes indicates a relative enhanced contribution of the allenylidene form in the organometallic compounds in comparison to the ethynyl ligands, in particular for Ru and Fe complexes:

$$[M]-C{\equiv}C-th-NO_2 \leftrightarrow [M]^+{=}C{=}C{=}th{=}NO_2{}^-$$
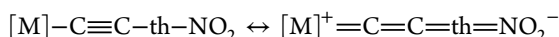
The contribution of the allenylidene form in the ground state has already been suggested by NMR spectroscopic data (see above). The overall data suggest an enhanced ground-state polarization due to an increasing of the donor−acceptor strength, i.e., the better Ru(II) and Fe(II) electron-donor organometallic moiety (compared to H in acetylide ligands) can form a very effective push−pull system in combination with acceptor nitro substituent in the thiophene acetylide chromophore.

In order to achieve a deep knowledge of the relevant electronic transitions involved, which can be helpful in the further discussion of the experimental first hyperpolarizabilities, we performed TDDFT calculations in the model complexes (TDDFT calculations of thiophene ligands $HC{\equiv}C$-$\{C_4H_2S\}_nNO_2$ are also included for comparison). The energies, oscillator strengths, and compositions of the main electronic transitions, in terms of the contributions of groups of atoms involved, are given in Table 5. The results show that, in general, TDDFT calculations overestimate the energy of the ETs for the studied complexes, in particular for **1′Fe**, in comparison to experimental data. However, a reasonable accuracy was obtained for $HC{\equiv}C\{C_4H_2S\}_nNO_2$ ligands and for complexes with two thienyl rings. In spite of the differences in the ET energies, TDDFT calculations reproduce the number of ET bands in the experimental UV−vis spectra. As an example, the calculated spectrum for **2a′Ru**, which can be compared to the experimental spectrum for **2aRu** (Figure 1), is given in the Supporting Information (Figure S14).

The analysis of the orbitals mainly involved in the ETs of the studied model complexes, depicted in Figures 3 and 4, together with the TDDFT data given in Table 5, allows us to predict reliable assignments of the bands observed in UV−vis experimental spectra of the corresponding synthesized complexes (Table 2).

First, we will consider the attribution of the higher energy bands for the complexes, in the range λ 286−410 nm. On the basis of the DFT calculations on the model **1′Fe**, **1a′Ru**, **1b′Ru**, and **1′Ni** complexes, the CT processes observed experimentally in the corresponding synthesized complexes with one thiophene ring, **1Fe**, **1aRu**, **1bRu**, and **1Ni**, seem to be somewhat complex. For **1Fe** this band seems to clearly be a MLCT, for **1aRu** some contribution of an intraligand CT is predicted, in addition to the MLCT, for **1bRu** an internal electronic charge transfer occurring at the organometallic moiety could also contribute to this band, in addition to MLCT and ILCT character, and finally for **1Ni** the experimental band at λ 404 nm can be clearly assigned to MLCT and the band at λ 286 nm can be assigned mainly to internal transitions occurring at the organometallic moiety together with some LMCT contribution. Considering the complexes with two thiophene rings, the experimental high-energy bands for **2bRu** and **2Ni** can be assigned to purely MLCT (on the basis of the DFT
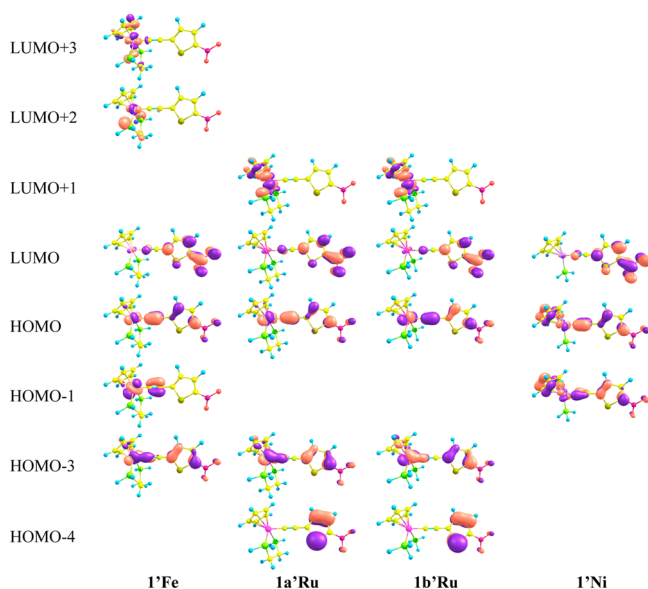

Figure 3. Representation of the main orbitals involved in electronic transitions of the complexes **1′Fe**, **1a′Ru**, **1b′Ru**, and **1′Ni**.
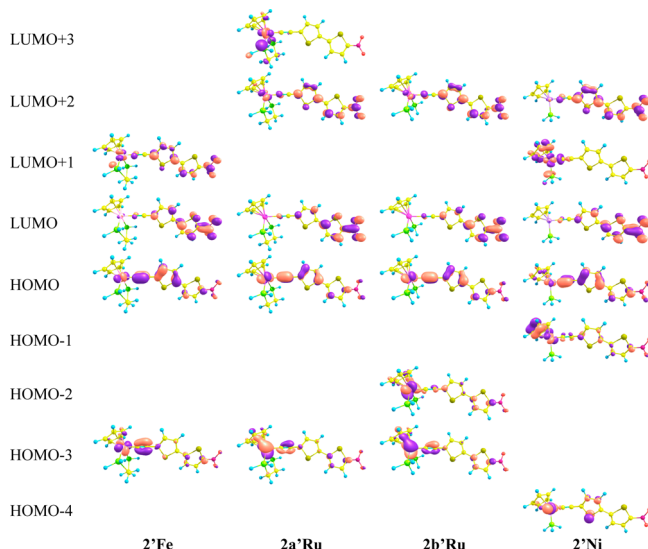

Figure 4. Representation of the main orbitals involved in electronic transitions of the complexes **2′Fe**, **2a′Ru**, **2b′Ru**, and **2′Ni**.

calculations on the model complexes **2b′Ru** and **2′Ni**, respectively), whereas for **2Fe** and **2aRu** the theoretical calculations on the corresponding models **2′Fe** and **2a′Ru** predict some contribution of internal charge transfer occurring at the organometallic moiety, in addition to the MLCT character.

In view of the second-order NLO properties it is important to consider the lower energy charge transfer excitations in some detail. For the synthesized Fe and Ru complexes with one thiophene ring, **1Fe**, **1aRu**, and **1bRu**, the experimental broad absorption band could be due to the existence of two CT contributions closer in energy, as predicted by TDDFT calculations (468 and 452 nm for **1′Fe**, 470 and 451 nm for **1′Ru**, and 473 and 446 nm for **1b′Ru**). This band can be viewed mainly as MLCT from the organometallic moiety to the NO_2 group, as expected considering the donor and acceptor character of the organometallic fragments and the nitro group,

respectively. In addition, the thiophene ring linked to the acetylide group (labeled T1 in Table 5) acts as a donor during charge transfer, as in the $HC≡C\{C_4H_2S\}NO_2$ ligand, and thus some contribution of ILCT character is observed. For these compounds, an electronic charge transfer within the organometallic fragment could also contribute to this band. In fact, TDDFT calculations revealed that the phosphane coligand also increases its electronic density during the excitation. For Ru complexes, in addition to the phosphane coligands, the Cp ring also slightly participates in this charge transfer process. In either case, the electronic transfer from the organometallic moiety to the acceptor NO_2 group during excitation is dominant for all complexes (ca. 60−80%). In contrast to that found for Fe and Ru complexes, in the synthesized nickel compound **1Ni** only one excitation is predicted, according to the calculations on the model complex **1′Ni**. This band can be assigned clearly to a MLCT, since the TDDFT results show that both NO_2 and the thiophene ring increase their electronic density during the transfer and the phosphane coligand seems not to participate in the process. In addition, the Cp ring has an active involvement as a donor in this electronic transition. Opposite to what was found for the synthesized **1Fe**, **1aRu**, and **1bRu**, in the case of complexes with two thiophene rings, and according to the calculations in the model complexes **2′Fe**, **2a′Ru**, **2b′Ru**, only one excitation is predicted and no contribution of the phosphane coligands and/or Cp ring as acceptors during the electronic transitions is observed. To a moderate extent, phosphane coligands and the Cp ring in fact act as electron donors during the CT process instead of electron acceptors. Thus, the experimental band for these complexes can be viewed to have higher MLCT character, in comparison to those for the **1Fe**, **1aRu**, and **1bRu** counterparts, in addition to the contribution of some internal electronic density transfer within the acetylide chromophore. The MLCT character is the result of a CT from the "CpM(PP)(C≡C)" fragment to the T2-NO_2 moiety and contributes ca. of 80% to the overall charge transfer process. The remaining charge transfer has an intraligand component and, as for the synthesized **1Fe**, **1aRu**, and **1bRu**, corresponds to the transfer of electronic density from the thiophene ring T1 (see Table 5) to the T2-NO_2 moiety. This ILCT contribution resembles the character of the CT occurring at the ligand $HC≡C\{C_4H_2S\}_2NO_2$, according to the TDDFT calculations. In the case of the ligand, T1 strongly decreases its electronic density during the excitation (Table 5). For the complexes, however, the participation of T1 is reduced at the expense of the organometallic moiety that plays an important role as a donor on the overall charge transfer process. In the case of the synthesized complex **2Ni**, the experimental absorption band ($λ$ 506 nm) can consist of two CT contributions closer in energy, as predicted by TDDFT calculations on the model complex **2′Ni** (521 and 510 nm). The CT process is somewhat complex, but the overall behavior resembles that found for **1Fe**, **1aRu**, and **1bRu**: i.e., in addition to the MLCT and ILCT character, an electronic charge transfer to the phosphane coligand could also contribute to this band. In either case, the electronic transfer to the T2-NO_2 moiety during excitation is dominant for this complex (ca. 75%). However, in comparison to what was found for **1Fe**, **1aRu**, and **1bRu**, a major contribution of a charge transfer occurring at the acetylide chromophore (ca. 60%) is predicted for **2Ni**, according to the theoretical calculations on the model **2′Ni** complex. Finally, as expected, the overall CT observed on the

complexes with two thiophene rings led to an increase of the electronic density mainly at the nitro group (ca. 60%).

The TDDFT data show that the chain lengthening of the chromophore led to a bathochromic effect on the calculated low-energy ETs for all of the model complexes (see Table 5), thus reproducing the experimental data (Table 2). An analysis of the energies of the frontier orbitals of the model complexes (Figure 5) shows that the introduction of a second thiophene
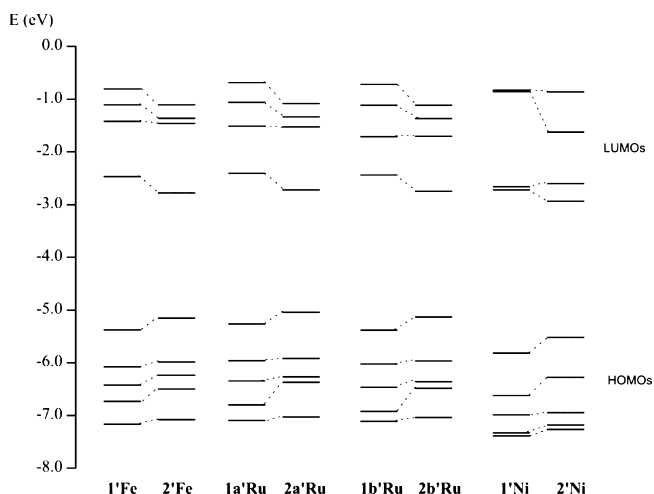

Figure 5. Energy levels of selected orbitals for the model complexes.

ring causes an increase of the energy of HOMOs and a decrease in the energy of LUMOs, leading to the expected reduction of the HOMO−LUMO gap and the observed bathochromic effect. The major contribution to the reduced HOMO−LUMO gap for iron and ruthenium complexes is due to the stabilization of LUMOs, whereas that for nickel is the destabilization of the HOMO. The overall result is an improved reduction effect on the HOMO−LUMO gap for the iron and ruthenium complexes in comparison to the nickel complexes.

Electrochemical Studies. In order to get an insight on the electron richness of the organometallic fragment and the coordinated chromophores, the electrochemical behavior of all complexes was studied by cyclic voltammetry in dichloromethane and acetonitrile, between the limits imposed by the solvents. As an example, the electrochemical response for **1bRu** in dichloromethane is shown in Figure 6, and the most relevant data for redox changes exhibited by all the complexes in
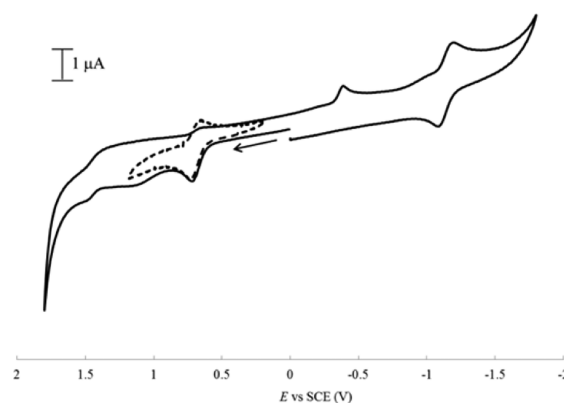

Figure 6. Cyclic voltamogramm of **1bRu** (−) showing the isolated oxidative process (- - -) in dichloromethane (scan rate 200 mV s^{-1}).

dichloromethane and acetonitrile at a scan rate of 200 mV s^{-1} are summarized in Tables 6 and 7, respectively.

Table 6. Cyclic Voltammetric Data for Compounds 1Fe, 1aRu, 1bRu, 1Ni, 2Fe, 2aRu, 2bRu, and 2Ni in CH$_2$Cl$_2$[a]

compd	E_{pc} (V)	E_{pa} (V)	$E_{1/2}$ (V)	$E_{pa} - E_{pc}$ (mV)	i_{pc}/i_{pa}
1Fe		1.59			
	0.25	0.33	0.29	80	1.0
	−1.0	−1.10			
2Fe		1.60			
	0.10	0.20	0.15	100	1.0
	−1.08	−0.94		140	
1aRu		1.28			
	0.55	0.64	0.59	100	0.3
	−1.09				
	−1.33	−1.13			
1bRu		1.29			
	0.58	0.67	0.63	90	0.5
	−1.06				
	−1.24	−1.10		140	
2aRu		1.10			
	0.38	0.48	0.43	100	0.5
	−1.07				
2bRu		1.12			
	0.42	0.52	0.47	100	0.6
	−1.08				
1Ni		0.86			
	−1.17[b]	−0.99[b]			
2Ni		0.78			
	−1.07				

[a]All values vs SCE (ν = 200 mV s^{-1}). [b]Small waves.

Table 7. Cyclic Voltammetric Data for Compounds 1Fe, 1Ni, 2Fe, and 2Ni in NCMe[a]

compd	E_{pc} (V)	E_{pa} (V)	$E_{1/2}$ (V)	$E_{pa} - E_{pc}$ (mV)	i_{pc}/i_{pa}
1Fe	0.20	0.28	0.24	80	1.0
	−0.99				
	−1.19	−1.09	−1.14	100	0.9[b]
2Fe	0.07	0.16	0.12	90	1.0
	−0.77				
	−1.0	−0.88		140	
1Ni		0.73			
	−0.52				
	−1.08	−0.99	−1.03	120	0.6[b]
2Ni		0.72			
	−0.53				
	−1.09	−0.97	−1.03	120	0.8[b]

[a]All values vs SCE (ν = 200 mV s^{-1}). [b]i_{pa}/i_{pc}.

The main electrochemical behavior in dichloromethane is characterized by the presence of one oxidation process, whose reversibility depends on the organometallic fragment, and one irreversible reductive process. In general, the oxidation process is usually viewed as essentially involving the M^{II}/M^{III} couple, but in the present case it is also associated with the acetylide ligand. In fact, according to our DFT calculations the mixing of the metal and acetylide frontier orbitals leads to HOMOs with both metal-centered and acetylide ligand contributions (Figures 3 and 4). These results are in accordance the behavior found for several arylalkynyl complexes that have shown a significant participation of the acetylide ligand in the oxidation

process.[44−49] The data are consistent with an oxidation process sensitive to the variation of the organometallic moiety and the chain lengthening of the acetylide ligand. The relative oxidation potentials for iron ($E_{1/2}$ = 0.15−0.29 V), ruthenium ($E_{1/2}$ = 0.43−0.63 V), and nickel (E_{pa} = 0.78−0.86 V) complexes are in agreement with the expected ease of oxidation of the organometallic moiety ([Fe] > [Ru] > [Ni]), considering their electronic properties. In the case of ruthenium complexes, replacing 2 PPh$_3$ by DPPE gives an expected decrease of the oxidation potential (40 mV), in accordance with the relative donor strength of the phosphane coligands. The chain lengthening of the acetylide ligand leads to a significant decrease in oxidation potentials, with the most significant variation (140 mV) being for iron complexes. This trend is analogous to that observed for the related benzene-based acetylide iron(II),[20] ruthenium(II),[24,25] and nickel(II)[33] complexes and also for analogous iron(II)[16] and ruthenium(II)[15] nitrile compounds. These results confirm the evidence of the spectroscopic data discussed above: namely, the magnitude of the metal to ligand π back-donation, which was found to decrease as the chain lengthening increases. The reversibility of the oxidation process depends on the organometallic moiety: it is reversible or quasi-reversible for iron and ruthenium complexes and irreversible for nickel complexes. In the case of ruthenium complexes, the i_{pc}/i_{pa} ratio (in the range 0.3−0.6) suggests some instability of the 17e species [Ru (η^5-C$_5$H$_5$)-(PP)(C≡C{C$_4$H$_2$S}$_n$NO$_2$)]$^+$ at the electrode surface (Figure 6). Scan rate studies showed that the process became more reversible when the scan direction was immediately reversed after the oxidation potential for high scan rates (1000 mV s^{-1}). In contrast, for the lower scan rate (50 mV s^{-1}) the process became more irreversible (see the Supporting Information, Figure S15). This behavior can be associated with the formation of an unstable oxidized ruthenium species followed by fast decomposition. At higher scan rates, the scan direction was reversed before an appreciable amount of decomposition occurred. Furthermore, experiments performed at −20 °C also showed some improvement in the reversibility, the values of the i_{pc}/i_{pa} ratio being augmented to 0.5−0.8 (see the Supporting Information, Figure S16), which suggests that the lower temperature diminishes the kinetics of the decomposition process.

As mentioned above, all complexes show one redox process, in the range of −1.01 to −1.20 V, which can be assigned mainly to reduction at the nitro group of the coordinated acetylide. In fact, according to the DFT calculations discussed above, the LUMOs of the model complexes are mainly located at this group (Figures 3 and 4). It is well-known that HOMO−LUMO gaps from electrochemical data can be correlated with optical properties.[50−52] In the present study, care should be taken in the quantitative correlation between HOMO−LUMO gaps from electrochemical data and optical properties due to the quasi-reversible/irreversible nature of the redox processes. However, a trend seems to be found between the HOMO−LUMO gap and the lowest-energy band observed in UV−vis spectra: the sequence of nickel, ruthenium, and iron complexes and chain lengthening of the acetylide ligands leads to a decrease in the HOMO−LUMO gap.

In addition to the oxidation and reduction processes discussed above, one irreversible oxidation, with E_{pa} = 1.59−1.60 V (for iron complexes) and E_{pa} = 1.10−1.29 V (for ruthenium complexes) is also observed, probably due to an additional oxidation at the thiophene moiety. For compound

1bRu a small irreversible cathodic wave, with E_{pc} = ca. -0.5 V, is also present and is attributed to decomposition products originating at higher oxidation potentials. In fact, this process vanishes when the direction of the cyclic voltammogram scan is moved toward negative potentials before proceeding to the oxidation of the complex (see the Supporting Information, Figure S17).

The electrochemical experiments in acetonitrile showed the same general behavior that was observed in dichloromethane. The ruthenium complexes, however, decompose in this solvent in the presence of the supporting electrolyte, and no results are available for these complexes. The redox processes assigned to reduction of the coordinated acetylide ligands, in the range -0.95 to -1.14 V, became more reversible for iron and nickel complexes. No significant changes were observed in the reversibility of the oxidation process. For the studied complexes, the oxidation potential is lower in acetonitrile, which reflects a relative destabilization of the HOMOs in comparison to that observed in dichloromethane. On the other hand, reduction potentials are shifted to lower negative values in acetonitrile, which reveals the stabilization of the LUMOs. The overall result is that HOMO−LUMO gaps are lower in acetonitrile in comparison to those observed in dichloromethane. This trend seems to agree with the solvatochromic behavior of the lower-energy bands in UV−vis spectra (see above), where a bathochromic shift upon an increase in the polarity of the solvent was found.

Quadratic Hyperpolarizabilities. Experimental data for all complexes at 1500 nm obtained by hyper-Rayleigh scattering and two-level-model (TLM) corrected values are collected in Table 8, together with data for the previously reported benzene-based iron(II), ruthenium(II), and nickel(II) acetylide complexes and also for analogous iron(II) nitrile compounds for comparison. Relevant experimental spectroscopic data and static quadratic hyperpolarizabilities calculated by DFT on our chosen model complexes were also included.

Earlier studies on related benzene-based iron(II),[20] ruthenium(II)[24,25] and nickel(II)[33] acetylide complexes reported β values measured at 1064 nm that showed substantial resonance enhancement, due to the existence of an optical transition in the visible range, very close to the second harmonic at 532 nm. It is well-known that for a reliable comparison of β between different molecules, and for a comparison with theoretical values, it is important to correctly account for these resonance effects and extrapolate β to the static first hyperpolarizability. The simple two-level model (TLM)[29] is widely used in the literature for this purpose but ignores any kind of line-broadening mechanisms and is not applicable near resonance,[18,53] which points out the importance of an appropriate theoretical β dispersion model for a reliable extrapolation. Recently, a practical model for first hyperpolarizability dispersion, accounting for both homogeneous and inhomogeneous broadening effects, was proposed on the basis of the relation between absorption and HRS spectra from tunable wavelength HRS measurements.[54]

Considering the λ_{max} for the compounds studied in this work, very high resonance enhancements could be expected for β measurements at 1064 nm. Therefore, to avoid this situation, our HRS measurements here presented were performed at the higher fundamental wavelength of 1500 nm to avoid superposition of the UV−vis absorptions and the second harmonic signal (750 nm), thus leading to more reasonable results according to the TLM analysis. The use of the TLM formalism

Table 8. Quadratic Hyperpolarizabilities and Relevant Spectroscopic Data

compd[a]	λ_{exp} (nm) (ε (10^4 M^{-1} cm^{-1}))	β	β_{corr}[b]	β_0[g]	ref
1Fe	578 (1.3)	232	80	97[h]	
2Fe	613 (1.5)	434	120	325	
[Fe](C≡C-ph-NO$_2$)	504 (0.8)	1160[c]	92[c]		20
[Fe](C≡C-(ph)$_2$-NO$_2$)	479 (0.5)	1150[c]	174[c]		20
[Fe](N≡C-th-NO$_2$)$^+$PF$_6^-$	579 (sh)	255[d]	97[d]		16
[Fe](N≡C-(th)$_2$-NO$_2$)$^+$PF$_6^-$	535 (sh)	177[d]	82[d]		16
1aRu	517 (2.0)	326	151	99[i]	
1bRu	536 (2.2)	192	82	96	
2aRu	566 (2.8)	506	187	356	
2bRu	580 (2.4)	655	224	321	
[Ru](C≡C-ph-NO$_2$)	460 (1.1)[e]	468[c,e]	96[c,e]		25
[Ru](C≡C-(ph)$_2$-NO$_2$)	448 (1.6)[e]	560[c,e]	134[c,e]		25
[Ru](C≡C-ph-(E)-CH=CH-th-NO$_2$)	533 (2.4)[f]	294[d,f]	138[d,f]		22
[Ru](C≡C-th-(E)-CH=CH-ph-NO$_2$)	522 (3.4)[f]	333[d,f]	163[d,f]		22
[Ru](C≡C-ph- C≡C-th-NO$_2$)	505 (2.0)[f]	210[d,f]	109[d,f]		22
[Ru](C≡C-(th-(E)-CH=CH)$_2$-ph-NO$_2$)	536 (4.5)[f]	419[d,f]	195[d,f]		22
1Ni	484 (0.7), 404 (0.2)	331	173	81	
2Ni	506 (2.3)	363	175	242	
[Ni](C≡CC$_6$H$_4$NO$_2$)	439 (0.9)[e]	221[c,e]	59[c,e]		33
[Ni](C≡C{C$_6$H$_4$}$_2$NO$_2$)	413 (1.6)[e]	193[c,e]	65[c,e]		33

All measurements were performed in CHCl$_3$ solution except where otherwise indicated. The β values are expressed in units of 10^{-30} esu and were measured at 1500 nm (β_{1500}) except where otherwise indicated (experimental error 15%). [a]Abbreviations: [Fe], CpFeDPPE; [Ru], CpRu(PPh$_3$)$_2$; [Ni], CpNiPPh$_3$; ph, C$_6$H$_4$; th, C$_4$H$_2$S. [b]β corrected for resonance enhancement using the two-level model with $\beta_{corr} = \beta[1 - (2\lambda_{max}/\lambda_{HRS})^2][1 - (\lambda_{max}/\lambda_{HRS})^2]$ (damping factors not included). [c]β_{1064}. [d]β_{1550}. [e]In THF. [f]In CH$_2$Cl$_2$. [g]Static quadratic hyperpolarizability of the model complexes calculated by DFT (the β tensor components are shown in the Supporting Information). [h]Reference 23. [i]Reference 40.

for the compounds studied in this work should be questioned at this point. This model assumes that for the contribution to β only one excited state is coupled strongly enough to the ground state by the applied electric field, and only one tensor component dominates the second-order NLO response (i.e., an unidirectional charge-transfer transition). The computed values of static hyperpolarizabilities of our model complexes show that β_0 is clearly dominated by the tensor component along the charge transfer axis, β_{xxx} (the β tensor components are shown in the Supporting Information, Table S3). However, as discussed above, the low-energy bands of **1Fe**, **1aRu**, **1bRu**, and **2Ni** are quite broad, revealing the existence of two CT contributions close in energy, as predicted by the TDDFT calculations in the corresponding model complexes. In addition, non-negligible contributions to the optical nonlinearity could be present for all complexes originating in the higher energy bands in the range 304−410 nm. In fact, our TDDFT calculations showed that these bands can also be assigned

mainly to MLCT transitions, with the expected large change in dipole moment upon excitation (see Table 5). Thus, the TLM formalism should be used with caution for our studied complexes, in particular for **1Fe**, **1aRu**, **1bRu**, and **2Ni**. Probably, a description of β using the dispersion model proposed by Campo et al.[54] mentioned above could be an improvement to consider in future work.

Our first hyperpolarizability results show that β_{corr} follows the trend **1Fe** ≈ **1bRu** < **1aRu** ≈ **1Ni** for the complexes with one thiophene ring. This trend is somewhat surprising, in particular for **1Ni**. Indeed, studies on related benzene-based iron(II),[20] ruthenium(II)[24,25] and nickel(II)[33] acetylide complexes suggested that the more easily oxidizable iron and ruthenium complexes lead to higher quadratic hyperpolarizabilities. The corrected hyperpolarizability for **1Ni** is almost 3 times that of $[Ni(\eta^5\text{-}C_5H_5)(PPh_3)(C{\equiv}CC_6H_4NO_2)]$, and the corresponding values of **1Fe** and **1bRu**, whose relative magnitudes are within the experimental error, are comparable to those found for related benzene-based iron(II) and ruthenium(II) acetylide complexes and an iron thiophene nitrile derivative (see Table 8). According to TLM we would be expect a greater second-order NLO response for iron and ruthenium complexes, since they have higher oscillator strength at the main MLCT bands (**1Fe**, λ_{exp} 578 nm; **1bRu**, λ_{exp} 536 nm; **1aRu**, λ_{exp} 517 nm; **1Ni**, λ_{exp} 484 and 404 nm). Furthermore, according to the solvatochromic results a larger change in the dipole moment is also expected for the iron and ruthenium complexes (**1Fe**, **1bRu**, and **1aRu**). Therefore, this apparently contradictory trend was analyzed in light of TDDFT calculations. For **1Fe**, **1aRu**, and **1bRu**, the experimental broad absorption band could be due to the existence of two CT contributions closer in energy, as predicted by TDDFT calculations (Table 5). In addition to the main HOMO−LUMO character of the overall CT process, also some contribution of a HOMO-1 to LUMO+3 transition (for **1′Fe**) and HOMO to LUMO+1 transition (for **1a′Ru** and **1b′Ru**) could be present in the broad band observed in the experimental spectra. In the case of **1′Fe** this charge transfer is within the organometallic fragment, while for **1a′Ru** and **1b′Ru** the charge transfer has mainly LMCT character, as can be seen in the representation of the involved orbitals (Figure 3). The resulting CT process is, thus, somewhat complex and these additional transitions would weaken the charge transfer efficiency from the metal donor fragment to the NO_2 acceptor group (a better CT efficiency would be expected for a purely MLCT process). For **1Ni** a very broad and complex experimental band was observed with λ centered at 484 and 404 nm (Table 2). According to the TDDFT calculations on the model complex **1′Ni**, the lowest-energy band (λ 484 nm) and second band (λ 404 nm) can be attributed respectively to the single transitions HOMO → LUMO and HOMO-1 → LUMO, both clearly with a MLCT character (see Table 5 and Figure 3). Since they are relatively closer in energy, probably these two bands contribute to the observed hyperpolarizability for **1Ni** and the purely MLCT processes certainly lead to improved CT efficiency. Thus, the improved CT efficiency expected for **1Ni**, in comparison to that found for ruthenium and iron complexes, could help to explain the overall trend on the quadratic hyperpolarizabilities for the complexes with one thiophene ring.

The chain lengthening of the acetylide chromophores, with the introduction of one thiophene ring, leads to higher quadratic hyperpolarizabilities for all the complexes. The β_{corr} values are in the range of those observed in a series of

ruthenium acetylides with an end-capping nitro group and thienyl and benzene entities in the conjugation chain[22] and benzene-based ruthenium[25] and iron[20] acetylide complexes (Table 8). Our results also show that iron and ruthenium complexes are more sensitive to the extension of the aromatic system than the nickel analogues. This result agrees with the trend found for the relative influence of the chain lengthening of the acetylide ligand on the degree of π back-donation interaction (IR data), the bathochromic effect of the low-energy transition bands (UV−vis data), and oxidation potentials (electrochemical data). Thus, for the same organometallic fragment, higher hyperpolarizabilities are associated with complexes having higher electron density at the organometallic moiety and low-energy transition bands. In addition, a hyperchromic effect is observed for these bands, which could also contribute to the enhanced hyperpolarizabilities. Considering the relative magnitude of the quadratic hyperpolarizabilities for compounds with two thiophene rings, the data show that β and β_{corr} follow respectively the trends **2Ni** < **2Fe** < **2aRu** < **2bRu** and **2Fe** < **2Ni** ≈ **2aRu** ≈ **2bRu**. However, considering that β_{corr} values of **2aRu**, **2bRu**, and **2Ni** are almost within the experimental error, a coherent analysis of the results is not straightforward. Some evidence pointed out by theoretical calculations could give an insight into the behavior of quadratic hyperpolarizabilities presented by the complexes with two thiophene rings. For **2Fe**, **2aRu**, and **2bRu** the lowest-energy band, observed in UV−vis spectra, can be attributed to a single transition (HOMO → LUMO) with a pure MLCT character (see Table 5 and Figure 4), according to our TDDFT calculations for the respective model complexes **2′Fe**, **2a′Ru**, and **2b′Ru**. For this reason, the use of the TLM formalism seems to be reasonable for these complexes. In spite of the expected small change in the dipole moment upon excitation (according to the solvatochromic results) and the higher energy of the main bands in the UV−vis spectra of ruthenium complexes (λ_{exp} 566−580 nm) in comparison to the iron compound (λ_{exp} 616 nm), the quadratic hyperpolarizabilities for ruthenium complexes are higher. Probably the relative intensity of these bands also plays an important role. In fact, a larger oscillator strength was found for **2aRu** and **2bRu** ($\varepsilon = 2.8 \times 10^4$ and 2.4×10^4 M^{-1} cm^{-1}, respectively) in comparison to **2Fe** (1.5×10^4 M^{-1} cm^{-1}). Accordingly, **2bRu** has also a higher quadratic hyperpolarizability than **2aRu**. As discussed for the complexes with one thiophene ring, we cannot exclude the possibility of a contribution to the overall hyperpolarizability of the higher energy band observed in experimental UV−vis spectra for the complexes with two thiophene rings (λ 373−410 nm). It is interesting to note that, according to the TDDFT calculations on the model complexes, this band for **2aRu** could have a contribution of charge transfer within the organometallic fragment, since the phosphane coligand increases its electronic density upon excitation (Table 5; λ_{eg} 380 nm). This can lead to some hampering effect on the overall hyperpolarizability in comparison to that found for **2bRu**. According to theoretical calculations on the model complex **2b′Ru**, a charge transfer within the organometallic fragment seems to be absent, which could result in an overall efficiency for this complex in comparison to that found for **2aRu**. Remarkably, **2bRu** presents a value of the corrected hyperpolarizability ($\beta_{corr} = 224 \times 10^{-30}$ esu) that places this complex in the range found for the best values of β_{corr} reported in the literature for an organometallic compound with quadratic hyperpolarizabilities measured at 1500 nm.[4−7,9,10] In the case of **2Ni** the use of TLM analysis is

also deceiving, since our TDDFT calculations on the model complex **2'Ni** (Table 5) predicted a contribution of two electronic transitions closer in energy to the experimental lowest energy band. In addition to the HOMO → LUMO transition, the contribution of the HOMO-1, HOMO-4, and LUMO+1 orbitals to the charge transfer could lead to a hampering effect on the overall hyperpolarizability, since these orbitals are mainly centered at the organometallic fragment (Figure 4). In comparison to the behavior found for **1Ni**, where a high quadratic hyperpolarizability was found, this hampering effect could explain the small increase in β (and almost unchanged β_{corr}) with the chain lengthening of the acetylide chromophore for this organometallic moiety.

In our previous studies on oligo-thiophene nitrile iron complexes the resonant quadratic hyperpolarizabilities were found to increase with the chain lengthening of the chromophore.[16] The corrected values, however, were found to be practically independent of the number of thiophene units in the conjugated ligand. This constancy upon chain lengthening was explained in terms of a competition between the growing conjugation length, which tends to raise β, and a decrease of the CT efficiency, having a β lowering effect. In the case of the present thiophene acetylide complexes a better CT efficiency seems to be obtained upon chain lengthening. In fact, as was discussed, TDDFT calculations on the model complexes have shown that relevant optical transitions have clearly MLCT character and a large amount of charge is transferred from the organometallic moiety to the chromophore, in particular for the acceptor NO_2 group, which largely increases its electronic density upon excitation.

The DFT approach has been increasingly used to calculate static quadratic hyperpolarizabilities of organometallic complexes.[55−59] In recent studies we calculated the static quadratic hyperpolarizabilities of **1'Fe**[23] and **1a'Ru**[40] using the DFT/B3LYP level of theory, and now we have extended these calculations to the remaining model complexes using the same level of theory for comparison. We are not as interested in comparing the absolute values of calculated hyperpolarizabilities to the experimental values, only in the observed trends, since several approximations were used (model phosphane coligands, isolated molecules in the gas phase (cf. experimental data obtained in solution), calculated static-frequency quadratic hyperpolarizability, β_0, vs experimental β_{1500}). In comparison to experimental data, the accuracy of calculated hyperpolarizabilities using the same level of theory depends on the studied molecules. For instance, DFT/B3LYP was found to reproduce reasonably well experimental quadratic hyperpolarizabilities for iron and ruthenium sesquifulvalene complexes[58] but can significantly overestimate or underestimate quadratic hyperpolarizabilities of ferrocenyl derivatives.[55] Also, it is well-known that calculated hyperpolarizabilities strongly depend on the level of theory used.[59,60,55] The results show that the calculated β_0 overestimates the experimental β_{corr} values in most cases (only for **1aRu** and **1Ni** was an underestimation observed). It is difficult to compare the trend found experimentally to that observed from computed values, due to the fact that several compounds have experimental quadratic hyperpolarizabilities falling within the experimental error. The computed hyperpolarizabilities increase ca. 3.0−3.6 times upon chain lengthening of the acetylide chromophore, whereas experimentally this enhancing effect is slightly smaller (up to ca. 2.7 times), probably due to the overestimation of quadratic hyper-

polarizabilities from DFT calculations in complexes with extended π-conjugated systems.[60]

■ CONCLUSIONS

A series of mono(η^5-cyclopentadienyl)iron(II), -ruthenium(II) and -nickel(II) complexes with nitro-substituted thienyl acetylide ligands has been synthesized and fully characterized. The spectroscopic and cyclic voltammetric data suggest an improved coupling between the organometallic fragment and the conjugated thienyl acetylide ligands, in comparison to the previously reported parent benzene-based acetylides and thiophene nitrile complexes. TDDFT studies on model complexes allowed us to achieve a deep knowledge of the relevant electronic transitions involved, which was very helpful in the discussion of the experimental quadratic hyperpolarizabilities. These properties have been determined by HRS measurements at 1500 nm. It is well recognized that, as a general behavior, better electron donor/acceptors and chain lengthening of the conjugated chromophore in push−pull systems should lead to higher quadratic hyperpolarizabilities. However a complexity in the push−pull systems based on organometallic donor moieties was found in the present study. The results seem to indicate that the effectiveness of an organometallic donor on the second-order NLO properties depends on the chain lengthening of the conjugated chromophore: the nickel organometallic fragment originates an enhanced effect on the magnitude of quadratic hyperpolarizability for short-length acetylide chromophores, whereas iron and ruthenium have comparatively higher NLO merit for long-length chromophores. In other words, iron and ruthenium complexes seem to be more sensitive to the extension of the aromatic system than the nickel analogues. In particular, the existence of other electronic transitions in addition to the main MLCT can clearly control the effectiveness of the organometallic donors on the second-order NLO properties of these push−pull systems. This leads to a somewhat surprisingly high quadratic hyperpolarizability for **1Ni** in comparison with **1Fe**, **1aRu**, and **1bRu** in spite of the better donor properties of iron and ruthenium organometallic moieties. $[Ru(\eta^5\text{-}C_5H_5)(PPh_3)_2(C\equiv C\{C_4H_2S\}_2NO_2)]$ presents a value of the corrected hyperpolarizability (224×10^{-30} esu) which places this complex in the range found for the best values of β_{corr} reported in the literature.

■ EXPERIMENTAL SECTION

General Procedures. Syntheses were carried out under a nitrogen atmosphere using standard Schlenk techniques, and the solvents used were dried by standard methods.[61] Commercial reagents were used without further purification, except for copper iodide, which was dried and kept under nitrogen. Starting materials were prepared by following the methods described in the literature: $[Ru(\eta^5\text{-}C_5H_5)(PPh_3)_2Cl]$ and $[Ru(\eta^5\text{-}C_5H_5)(DPPE)Cl]$,[62] $[Fe(\eta^5\text{-}C_5H_5)(DPPE)I]$,[16] $[Ni(\eta^5\text{-}C_5H_5)(PPh_3)Cl]$.[63] 2-(5-Bromothiophen-2-yl)-5-nitrothiophene was prepared by bromination of 2-nitro-5-(thiophen-2-yl)thiophene with NBS according to the general method described in the literature.[64] 2-Nitro-5-(thiophen-2-yl)thiophene was prepared by nitration of 2,2'-bithiophene with Claycop according to general procedures.[65] The syntheses of trimethyl((5-nitrothiophen-2-yl)ethynyl)silane (**1**),[34] 2-ethynyl-5-nitrothiophene (**1'**),[34] trimethyl((5'-nitro-2,2'-bithiophen-5-yl)ethynyl)silane (**2**),[30] 5-ethynyl-5'-nitro-2,2'-bithiophene (**2'**),[30] and $Ru(\eta^5\text{-}C_5H_5)(PPh_3)_2(C\equiv C\{C_4H_2S\}NO_2)$ (**1bRu**)[34] were previously reported. In this work we used some modifications for the preparation of **1**, **1'**, **2**, and **2'** (see details below): trimethyl((5-nitrothiophen-2-yl)ethynyl)silane (**1**) was prepared using $Pd(PPh_3)_2Cl_2$ as precatalyst

instead of Pd(OAc)$_2$/PPh$_3$;[34] trimethyl((5′-nitro-2,2′-bithiophen-5-yl)ethynyl)silane (**2**) was prepared from the bromo-substituted precursor instead of the reported iodo derivative[30] using standard procedures; a different deprotection procedure for the trimethylsilane group was used for obtaining 2-ethynyl-5-nitrothiophene (**1′**)[34] and 5-ethynyl-5′-nitro-2,2′-bithiophene (**2′**).[30] ^{1}H, ^{13}C, and ^{31}P NMR spectra were recorded on a Bruker Avance 400 spectrometer at probe temperature using CDCl$_3$ or (CD$_3$)$_2$CO as solvents. The ^{1}H and ^{13}C chemical shifts (s, singlet; d, doublet; t, triplet; m, multiplet for ^{1}H) are reported in parts per million (ppm) downfield from the residual solvent peak, and the ^{31}P NMR spectra are reported in ppm downfield from the external standard 85% H$_3$PO$_4$. Coupling constants are reported in Hz. Spectral assignments follow the numbering scheme shown in Scheme 1 and are attributed using HMBC, HMQC, and COSY NMR techniques. FT-IR spectra were recorded with a Perkin-Elmer Paragon 1000 PC spectrophotometer as dry KBr pellets (only significant bands are cited). UV–vis spectra were recorded with a Termo Electron, Nicolet Evolution 300 instrument, in dried solvents in the range of 200−1000 nm. Elemental analyses were obtained at our laboratories (Laboratório de Análises, Instituto Superior Técnico), using a Fisons Instruments EA1108 system. Data acquisition, integration, and handling were performed using a PC with the software package EAGER-200 (Carlo Erba Instruments).

Synthesis of Me$_3$SiC≡C{C$_4$H$_2$S}NO$_2$ (1). 5-Bromo-2-nitrothiophene (1.0 g; 5 mmol) was dissolved in THF (10 mL). Pd(PPh$_3$)$_2$Cl$_2$ (0.07 g, 0.10 mmol), CuI (0.019 g, 0.10 mmol), and NEt$_3$ (1.2 g, 7.9 mmol) were added. A solution of ethynyltrimethylsilane (0.55 g, 5.5 mmol) in THF (20 mL) was added dropwise, and the mixture was stirred for 2 h. The resultant dark brown suspension was filtered, and the solid was washed with dichloromethane (10 mL). The combined THF and dichloromethane solvents were evaporated under vacuum, and the resultant brown residue was then chromatographed on silica gel. Elution with petroleum ether 40−60/Et$_2$O (9/1) gave a yellow band from which microcrystalline trimethyl((5-nitrothiophen-2-yl)ethynyl)silane was isolated in 76% yield (0.856 g). ν(KBr)/cm^{-1}: 1345s and 1523s (NO$_2$), 2141m (C≡C). ^{1}H NMR (CDCl$_3$): δ/ppm 0.28 (s, 9H, CH$_3$), 7.11 (d, 1H, $^3J_{HH}$ = 4.0 Hz, H4), 7.78 (d, 1H, $^3J_{HH}$ = 4.4 Hz, H5). ^{13}C NMR (CDCl$_3$): δ/ppm 0.21 (CH$_3$), 95.36 (C2), 105.42 (C1), 128.32 (C5), 130.61 (C3), 131.54 (C4), 150.76 (C6). UV–vis (CHCl$_3$): λ$_{max}$/nm (ε/10^4 M^{-1} cm^{-1}) 356 (1.1).

Synthesis of HC≡C{C$_4$H$_2$S}NO$_2$ (1′). Compound **1** (0.338 g, 1.5 mmol) was dissolved in methanol (10 mL). Ammonium fluoride (0.061 g, 1.65 mmol) was added. After the mixture was stirred at room temperature for 2 h, the solvent was removed under vacuum to give a brown residue. The solid was washed with petroleum ether 40−60 and the solvent evaporated to give the desired product as a light yellow microcrystalline powder in 72% yield (0.165 g). ν(KBr)/cm^{-1}: 1341s and 1528s (NO$_2$), 2101m (C≡C). ^{1}H NMR (CDCl$_3$): δ/ppm 3.57 (s, 1H, C≡C*H*), 7.17 (d, 1H, $^3J_{HH}$ = 4.0 Hz, H4), 7.80 (d, 1H, $^3J_{HH}$ = 4.0 Hz, H5). ^{1}H NMR ((CD$_3$)$_2$CO): δ/ppm 4.47 (s, 1H, C≡C*H*), 7.41 (d, 1H, $^3J_{HH}$ = 4.0 Hz, H4), 8.00 (d, 1H, $^3J_{HH}$ = 4.0 Hz, H5). ^{13}C NMR (CDCl$_3$): δ/ppm 75.13 (C2), 86.04 (C1), 128.12 (C5), 129.15 (C3), 132.17 (C4), 151.29 (C6). ^{13}C NMR ((CD$_3$)$_2$CO): δ/ppm 74.48 (C2), 87.45 (C1), 128.79 (C3), 129.08 (C5), 133.04 (C4), 147.75 (C6). UV–vis (CHCl$_3$): λ$_{max}$/nm (ε/10^4 M^{-1} cm^{-1}) 346 (0.8).

Synthesis of Me$_3$SiC≡C{C$_4$H$_2$S}$_2$NO$_2$ (2). 2-(5-Bromothiophen-2-yl)-5-nitrothiophene (0.14 g, 0.5 mmol) was dissolved in THF (5 mL). Pd(PPh$_3$)$_2$Cl$_2$ (0.017 g, 0.025 mmol), CuI (0.008 g, 0.04 mmol), and NEt$_3$ (0.3 mL, 1.98 mmol) were added. A solution of ethynyltrimethylsilane (0.1 g, 1.0 mmol) in THF (10 mL) was added dropwise, and the mixture was stirred overnight. The solvent was evaporated under vacuum, and the resultant brown residue was then chromatographed on silica gel. Elution with petroleum ether 40−60/Et$_2$O (9/1) gave an orange band from which trimethyl((5′-nitro-2,2′-bithiophen-5-yl)ethynyl)silane was isolated as an orange powder in 70% yield (0.108 g). ν(KBr)/cm^{-1}: 1327s and 1515s (NO$_2$), 2141m (C≡C). ^{1}H NMR (CDCl$_3$): δ/ppm 0.27 (s, 9H, CH$_3$), 7.08 (d, 1H, $^3J_{HH}$ = 4.4 Hz, H8), 7.18 (d, 1H, $^3J_{HH}$ = 4.0 Hz, H4), 7.20 (d, 1H, $^3J_{HH}$ = 3.6 Hz, H5), 7.85 (d, 1H, $^3J_{HH}$ = 4.4 Hz, H9). ^{13}C NMR (CDCl$_3$): δ/ppm 0.15 (CH$_3$), 96.36 (C2), 102.55 (C1), 122.84 (C8), 125.68

(C6), 126.65 (C5), 129.71 (C9), 133.71 (C4), 135.77 (C3), 144.08 (C7), 149.73 (C10). UV–vis (CHCl$_3$): λ$_{max}$/nm (ε/10^4 M^{-1} cm^{-1}) 416 (2.2).

Synthesis of HC≡C{C$_4$H$_2$S}$_2$NO$_2$ (2′). Compound **2** (0.25 g, 0.8 mmol) was dissolved in methanol (70 mL). Ammonium fluoride (0.033 g, 0.88 mmol) was added. After the mixture was stirred at room temperature for 2 h, an orange solid precipitated. After 3 h of additional stirring, the solvent was removed under vacuum to give an orange solid. The solid was washed with dichloromethane and the solvent evaporated to give the desired product as a light orange solid in 77% yield (0.145 g). ν(KBr)/cm^{-1}: 1325s and 1511s (NO$_2$), 2096m (C≡C). ^{1}H NMR (CDCl$_3$): δ/ppm 3.50 (s, 1H, CH), 7.09 (d, 1H, $^3J_{HH}$ = 4.4 Hz, H8), 7.21 (d, 1H, $^3J_{HH}$ = 4.0 Hz, H4), 7.23 (d, 1H, $^3J_{HH}$ = 4.0 Hz, H5), 7.85 (d, 1H, $^3J_{HH}$ = 4.0 Hz, H9). ^{1}H NMR ((CD$_3$)$_2$CO): δ/ppm 4.27 (s, 1H, CH), 7.39 (d, 1H, $^3J_{HH}$ = 4.0 Hz, H4), 7.44 (d, 1H, $^3J_{HH}$ = 4.0 Hz, H8), 7.56 (d, 1H, $^3J_{HH}$ = 4.0 Hz, H5), 8.03 (d, 1H, $^3J_{HH}$ = 4.0 Hz, H9). ^{13}C NMR (CDCl$_3$): δ/ppm 75.98 (C2), 84.09 (C1), 123.01 (C8), 124.33 (C3), 126.09 (C4), 129.61 (C9), 134.20 (C5), 136.16 (C6), 143.74 (C7), not attributed (C10). ^{13}C NMR ((CD$_3$)$_2$CO): δ/ppm 76.54 (C2), 86.30 (C1), 123.03 (C3), 124.10 (C4), 128.09 (C8), 131.30 (C9), 135.57 (C5), 136.92 (C6), 143.18 (C7), 150.81 (C10). UV–vis (CHCl$_3$): λ$_{max}$/nm (ε/10^4 M^{-1} cm^{-1}) 410 (1.3).

Synthesis of Fe(η^5-C$_5$H$_5$)(DPPE)(C≡C{C$_4$H$_2$S}NO$_2$) (1Fe). To a suspension of Fe(η^5-C$_5$H$_5$)(DPPE)I (0.40 g, 0.62 mmol) and **1′** (0.11 g, 0.65 mmol) in methanol (30 mL) was added NH$_4$PF$_6$ (0.11 g, 0.68 mmol), and the mixture was refluxed for 2 h and then cooled. A solution of NaOMe in methanol (7.4 mL, 0.1 M) was added, and the mixture was stirred for 1 h at room temperature. The solvent was removed under vacuum, and the resultant solid residue was then chromatographed on flash silica gel. Elution with *n*-hexane/Et$_2$O (1/1) gave a dark blue band from which the desired compound was isolated as a dark blue solid in 76% yield (0.32 g). ν(KBr)/cm^{-1}: 1421s and 1292s (NO$_2$), 2005m (C≡C). ^{1}H NMR ((CD$_3$)$_2$CO): δ/ppm 2.51 (m, 2H, CH$_2$-DPPE), 2.63 (m, 2H, CH$_2$-DPPE), 4.39 (s, 5H, C$_5$H$_5$), 5.92 (d, 1H, $^3J_{HH}$ = 4.6 Hz, H4), 7.60 (d, 1H, $^3J_{HH}$ = 4.6 Hz, H5), 7.34−7.44 and 7.90 (m, 20H, H-Ph). ^{13}C NMR ((CD$_3$)$_2$CO): δ/ppm 30.41 (CH$_2$-DPPE), 81.24 (s, C$_5$H$_5$), 118.52 (C2), 125.37 (C4), 128.68 (t, $^2J_{CP}$ = 9.0 Hz, C$_{ortho}$-Ph), 129.13 (t, $^2J_{CP}$ = 8.1 Hz, C$_{ortho}$-Ph), 130.40 (s, C$_{para}$-Ph), 131.67 (C5), 131.69 (s, C$_{para}$-Ph), 132.51 (t, $^3J_{CP}$ = 8.8 Hz, C$_{meta}$-Ph), 134.24 (t, $^3J_{CP}$ = 8.8 Hz, C$_{meta}$-Ph), 136.45 (t, $^1J_{CP}$ = 13.6 Hz, C$_{ipso}$-Ph), 138.18 (t, $^1J_{CP}$ = 14.9 Hz, C$_{ipso}$-Ph), 140.05 (C3), 141.90 (t, $^2J_{CP}$ = 28.5 Hz, C1), 143.34 (C6). ^{31}P NMR ((CD$_3$)$_2$CO): δ/ppm 103.93 (s, 2P-DPPE). UV–vis (CHCl$_3$): λ$_{max}$/nm (ε/10^4 M^{-1} cm^{-1}) 578 (1.3). Anal. Calcd for C$_{37}$H$_{31}$FeNO$_2$P$_2$S: C, 66.18; H, 4.65; N, 2.09; S, 4.78. Found: C, 65.80; H, 5.00; N, 1.99; S, 5.00.

Synthesis of Fe(η^5-C$_5$H$_5$)(DPPE)(C≡C{C$_4$H$_2$S}$_2$NO$_2$) (2Fe). To a suspension of Fe(η^5-C$_5$H$_5$)(DPPE)I (0.40 g, 0.62 mmol) and **2′** (0.16 g, 0.68 mmol) in methanol (50 mL) was added NH$_4$PF$_6$ (0.11 g, 0.68 mmol), and the mixture was refluxed for 3 h and then cooled. A solution of NaOMe in methanol (7.4 mL, 0.1 M) was added, and the mixture was stirred for 1 h at room temperature. The solvent was removed under vacuum, and the resultant solid residue was then flash chromatographed on silica gel. Elution with *n*-hexane/Et$_2$O (2/3) gave a dark blue band from which the desired compound was isolated as a blue-purple solid in 78% yield (0.36 g). ν(KBr)/cm^{-1}: 1422s and 1298s (NO$_2$), 2024m (C≡C). ^{1}H NMR ((CD$_3$)$_2$CO): δ/ppm 2.45 (m, 2H, CH$_2$-DPPE), 2.62 (m, 2H, CH$_2$-DPPE), 4.31 (s, 5H, C$_5$H$_5$), 6.00 (d, 1H, $^3J_{HH}$ = 3.9 Hz, H4), 6.99 (d, 1H, $^3J_{HH}$ = 4.4 Hz, H8), 7.17 (d, 1H, $^3J_{HH}$ = 3.9 Hz, H5), 7.88 (d, 1H, $^3J_{HH}$ = 3.9 Hz, H9), 7.33−7.46 and 7.94 (m, 20H, H-Ph). ^{13}C NMR ((CD$_3$)$_2$CO): δ/ppm 29.84 (CH$_2$-DPPE), 80.41 (s, C$_5$H$_5$), 115.24 (C2), 121.26 (C8), 126.73 (C4), 127.45 (C6), 128.42 (C5), 128.46 (t, $^3J_{CP}$ = 9.0 Hz, C$_{meta}$-Ph), 128.89 (t, $^2J_{CP}$ = 9.0 Hz, C$_{ortho}$-Ph), 129.84 (s, C$_{para}$-Ph), 130.07 (s, C$_{para}$-Ph), 131.56 (C9), 132.47 (t, $^2J_{CP}$ = 8.5 Hz, C$_{ortho}$-Ph), 134.29 (t, $^2J_{CP}$ = 8.6 Hz, C$_{meta}$-Ph), 135.42 (C3), 138.34 (t, $^1J_{CP}$ = 49.5 Hz, C$_{ipso}$-Ph), 142.28 (t, $^2J_{CP}$ = 31.3 Hz, C1), 147.36 (C7), 152.41 (C10). ^{31}P NMR ((CD$_3$)$_2$CO): δ/ppm 104.5 (s, 2P-DPPE). UV–vis (CHCl$_3$):

λ_{max}/nm ($\varepsilon/10^4$ M^{-1} cm^{-1}) 613 (1.5). Anal. Calcd for C$_{41}$H$_{33}$FeNO$_2$P$_2$S$_2$: C, 65.34; H, 4.41; N, 1.86; S, 8.51. Found: C, 64.80; H, 4.40; N, 1.90; S, 9.00.

Synthesis of Ru(η^5-C$_5$H$_5$)(DPPE)(C≡C{C$_4$H$_2$S}NO$_2$) (1aRu). To a suspension of Ru(η^5-C$_5$H$_5$)(DPPE)Cl (0.30 g, 0.5 mmol) and **1** (0.13 g, 0.58 mmol) in methanol (30 mL) was added KF (0.045 g, 0.75 mmol), and the mixture was refluxed for 4 h. The solvent was removed under vacuum, and the resultant solid residue was then flash chromatographed on silica gel. Elution with *n*-hexane/Et$_2$O (1/1) gave a purple band, from which the desired compound was isolated as a purple solid in 70% yield (0.25 g). ν(KBr)/cm^{-1}: 1297s and 1419s (NO$_2$), 2023m (C≡C). ^{1}H NMR (CDCl$_3$): δ/ppm 2.33 (m, 2H, CH$_2$-DPPE), 2.58 (m, 2H, CH$_2$-DPPE), 4.84 (s, 5H, C$_5$H$_5$), 5.81 (d, 1H, $^3J_{HH}$ = 4.4 Hz, H4), 7.53 (d, 1H, $^3J_{HH}$ = 4.4 Hz, H5), 7.30−7.42 and 7.80 (m, 20H, H-Ph). ^{13}C NMR (CDCl$_3$): δ/ppm 28.26 (t, $^1J_{CP}$ = 47.2, CH$_2$-DPPE), 83.05 (s, C$_5$H$_5$), 108.76 (C2), 125.47 (C4), 127.96 (t, $^3J_{CP}$ = 27.2 Hz, C$_{meta}$-Ph), 128.13 (t, $^3J_{CP}$ = 25.0 Hz, C$_{meta}$-Ph), 129.33 (s, C$_{para}$-Ph), 129.80 (s, C$_{para}$-Ph), 130.76 (C5), 131.41 (t, $^2J_{CP}$ = 28.8 Hz, C$_{ortho}$-Ph), 133.38 (t, $^2J_{CP}$ = 27.6 Hz, C$_{ortho}$-Ph), not attributed (C$_{ipso}$-Ph), 140.51 (C3), 142.43 (C6), 143.36 (t, $^2J_{CP}$ = 21.0 Hz, C1). ^{31}P NMR (CDCl$_3$): δ/ppm 84.62 (s, 2P-DPPE). UV−vis (CHCl$_3$): λ_{max}/nm ($\varepsilon/10^4$ M^{-1} cm^{-1}) 517 (2.0). Anal. Calcd for C$_{37}$H$_{31}$NO$_2$P$_2$RuS: C, 62.00; H, 4.36; N, 1.95; S, 4.47. Found: C, 62.12; H, 4.60; N, 1.90; S, 4.30.

Synthesis of Ru(η^5-C$_5$H$_5$)(DPPE)(C≡C{C$_4$H$_2$S}$_2$NO$_2$) (2aRu). Ru(η^5-C$_5$H$_5$)(DPPE)Cl (0.15 g, 0.25 mmol) and **2** (0.08 g, 0.26 mmol) were suspended in methanol (40 mL), and a few drops of dichloromethane were added to ensure complete solubilization. After the mixture was stirred at room temperature for 2.5 h and refluxed for an additional 3.5 h, TlPF$_6$ (0.09 g, 0.27 mmol) was added and, immediately, the yellow vinylidene derivative [Ru(η^5-C$_5$H$_5$)(DPPE)(=C=CH{C$_4$H$_2$S}$_2$NO$_2$)][PF$_6$] precipitated. The solid was filtered, washed with diethyl ether, and dried under vacuum. Subsequent redissolution in methanol (30 mL) with 5% acetone and addition of sodium methoxide (0.016 g, 0.3 mmol) afforded a dark purple solution. The mixture was stirred for 1 h at room temperature. The solvents were removed under vacuum, and the resultant solid residue was then flash chromatographed on silica gel. Elution with *n*-hexane/Et$_2$O (1/1) gave a purple band, from which the desired compound was isolated as a purple solid in 72% yield (0.14 g). ν(KBr)/cm^{-1}: 1291s and 1412s (NO$_2$), 2037m (C≡C). ^{1}H NMR (CDCl$_3$): δ/ppm 2.26 (m, 2H, CH$_2$-DPPE), 2.68 (m, 2H, CH$_2$-DPPE), 4.83 (s, 5H, C$_5$H$_5$), 5.63 (d, 1H, $^3J_{HH}$ = 3.9 Hz, H4), 6.81 (d, 1H, $^3J_{HH}$ = 4.5 Hz, H8), 7.00 (d, 1H, $^3J_{HH}$ = 3.9 Hz, H5), 7.76 (d, 1H, $^3J_{HH}$ = 4.5 Hz, H9), 7.32−7.34 and 7.56 (m, 20H, H-Ph). ^{13}C NMR (CDCl$_3$): δ/ppm 27.69 (t, $^1J_{CP}$ = 50.0 Hz, CH$_2$-DPPE), 83.78 (s, C$_5$H$_5$), 119.17 (C8), 119.66 (C4), 125.82 (C6), 127.55 (C2), 127.79 (t, $^3J_{CP}$ = 17.4 Hz, C$_{meta}$-Ph), 128.01 (t, $^3J_{CP}$ = 18.5 Hz, C$_{meta}$-Ph), 129.07 (s, C$_{para}$-Ph), 126.90 (C5), 129.11 (s, C$_{para}$-Ph), 130.81 (C9), 132.13 (t, $^2J_{CP}$ = 20.0 Hz, C$_{ortho}$-Ph), 132.26 (t, $^2J_{CP}$ = 19.1 Hz, C$_{ortho}$-Ph), 138.41 (t, $^1J_{CP}$ = 85.9 Hz, C$_{ipso}$-Ph), 141.28 (C7), 141.76 (C3), 145.25 (t, $^2J_{CP}$ = 105.6 Hz, C1), 149.57 (C10). ^{31}P NMR (CDCl$_3$): δ/ppm 85.33 (s, 2P-DPPE). UV−vis (CHCl$_3$): λ_{max}/nm ($\varepsilon/10^4$ M^{-1} cm^{-1}) 566 (2.8). Anal. Calcd for C$_{41}$H$_{33}$NO$_2$P$_2$RuS$_2$: C, 61.64; H, 4.16; N, 1.75; S, 8.03. Found: C, 61.20; H, 4.30; N, 1.70; S, 8.00.

Synthesis of Ru(η^5-C$_5$H$_5$)(PPh$_3$)$_2$(C≡C{C$_4$H$_2$S}NO$_2$) (1bRu). To a solution of Ru(η^5-C$_5$H$_5$)(PPh$_3$)$_2$Cl (0.11 g, 0.15 mmol) and **1** (0.036 g, 0.16 mmol) in methanol (30 mL) was added KF (0.022 g, 0.30 mmol), and the mixture was refluxed for 3 h. The solvent was removed under vacuum, and the resultant solid residue was then flash chromatographed on silica gel. Elution with *n*-hexane/Et$_2$O (1/1) gave a purple band, from which the desired compound was isolated as a purple microcrystalline solid in 77% yield (0.10 g). ν(KBr)/cm^{-1}: 1294s and 1419s (NO$_2$), 2019m (C≡C). ^{1}H NMR (CDCl$_3$): δ/ppm 4.39 (s, 5H, C$_5$H$_5$), 6.39 (d, 1H, $^3J_{HH}$ = 4.2 Hz, H4), 7.78 (d, 1H, $^3J_{HH}$ = 4.2 Hz, H5), 7.12−7.28 (m, 30H, H-PPh$_3$). ^{13}C NMR (CDCl$_3$): δ/ppm 86.10 (s, C$_5$H$_5$), 111.83 (C2), 125.38 (C4), 127.54 (t, $^3J_{CP}$ = 20.0 Hz, C$_{meta}$-PPh$_3$), 128.92 (s, C$_{para}$-PPh$_3$), 131.04 (C5), 133.10 (C1), 133.60 (t, $^2J_{CP}$ = 20.0 Hz, C$_{ortho}$-PPh$_3$), 137.94 (t, $^1J_{CP}$ = 88.0 Hz, C$_{ipso}$-PPh$_3$), 142.39 (C6), 143.00 (C3). ^{31}P NMR (CDCl$_3$): δ/ppm 49.94

(s, 2P-PPh$_3$). UV−vis (CHCl$_3$): λ_{max}/nm ($\varepsilon/10^4$ M^{-1}c m^{-1}) 536 (2.2). Anal. Calcd for C$_{47}$H$_{37}$NO$_2$P$_2$RuS: C, 66.97; H, 4.42; N, 1.66; S, 3.80. Found: C, 67.00; H, 4.50; N, 1.60; S, 4.00.

Synthesis of Ru(η^5-C$_5$H$_5$)(PPh$_3$)$_2$(C≡C{C$_4$H$_2$S}$_2$NO$_2$) (2bRu). To a suspension of Ru(η^5-C$_5$H$_5$)(PPh$_3$)$_2$Cl (0.27 g, 0.50 mmol) and **2** (0.17 g, 0.52 mmol) in methanol (30 mL) was added KF (0.14 g, 2.4 mmol), and the mixture was refluxed for 4.5 h. The solvent was removed under vacuum, and the resultant solid residue was then flash chromatographed on silica gel. Elution with *n*-hexane/Et$_2$O (1/1) gave a dark blue band, from which the desired compound was isolated as a dark blue solid in 54% yield (0.25 g). ν(KBr)/cm^{-1}: 1309s and 1431s (NO$_2$), 2037m (C≡C). ^{1}H NMR (CDCl$_3$): δ/ppm 4.36 (s, 5H, C$_5$H$_5$), 6.53 (d, 1H, $^3J_{HH}$ = 3.9 Hz, H4), 6.90 (d, 1H, $^3J_{HH}$ = 4.3 Hz, H8), 7.13−7.43 (m, 30H, H-PPh$_3$), 7.19 (d, 1H, $^3J_{HH}$ = 3.9 Hz, H5), 7.81 (d, 1H, $^3J_{HH}$ = 4.3 Hz, H9). ^{13}C NMR (CDCl$_3$): δ/ppm 85.67 (s, C$_5$H$_5$), 108.43 (C2), 120.25 (C8), 126.70 (C4), 127.41 (t, $^3J_{CP}$ = 17.5 Hz, C$_{meta}$-PPh$_3$), 127.92 (C5), 128.69 (s, C$_{para}$-PPh$_3$), 130.44 (C9), 133.70 (t, $^2J_{CP}$ = 19.7 Hz, C$_{ortho}$-PPh$_3$), 135.30 (C7), 137.94 (C6), 138.36 (t, $^1J_{CP}$ = 84.4 Hz, C$_{ipso}$-PPh$_3$), 140.21 (t, $^2J_{CP}$ = 83.1 Hz, C1), 146.80 (C3), 147.37 (C10). ^{31}P NMR (CDCl$_3$): δ/ppm 49.98 (s, 2P-PPh$_3$). UV−vis (CHCl$_3$): λ_{max}/nm ($\varepsilon/10^4$ M^{-1} cm^{-1}) 580 (2.4). Anal. Calcd for C$_{51}$H$_{39}$NO$_2$P$_2$RuS$_2$: C, 66.22; H, 4.25; N, 1.51; S, 6.93. Found: C, 66.44; H, 4.24; N, 1.53; S, 6.91.

Synthesis of Ni(η^5-C$_5$H$_5$)(PPh$_3$)(C≡C{C$_4$H$_2$S}NO$_2$) (1Ni). Ni(η^5-C$_5$H$_5$)(PPh$_3$)Cl (0.42 g, 1.0 mmol), **1′** (0.17 g, 1.10 mmol), and CuI (0.015 g, 0.08 mmol) were suspended in NEt$_3$/THF 4/1 (25 mL). After the mixture was stirred at room temperature for 16 h, the solvent was removed under vacuum and the resultant solid residue was extracted with dichloromethane and then flash chromatographed on silica gel. Elution with *n*-hexane/Et$_2$O (4/1) gave a red band, from which the desired compound was isolated as a wine red solid in 80% yield (0.47 g). ν(KBr)/cm^{-1}: 1339s and 1516s (NO$_2$), 2074m (C≡C). ^{1}H NMR (CDCl$_3$): δ/ppm 5.26 (s, 5H, C$_5$H$_5$), 6.17 (d, 1H, $^3J_{HH}$ = 4.2 Hz, H4), 7.53 (d, 1H, $^3J_{HH}$ = 4.2 Hz, H5), 7.39−7.47 and 7.60−7.69 (m, 15H, H-PPh$_3$). ^{13}C NMR (CDCl$_3$): δ/ppm 92.98 (s, C$_5$H$_5$), 111.35 (C2), 126.92 (C4), 128.42 (t, $^3J_{CP}$ = 10.5 Hz, C$_{meta}$-PPh$_3$), 130.56 (s, C$_{para}$-PPh$_3$), 129.36 (C5), 115.24 (d, $^2J_{CP}$ = 45.2 Hz, C1), 133.67 (t, $^2J_{CP}$ = 11.1 Hz, C$_{ortho}$-PPh$_3$), 133.22 (t, $^1J_{CP}$ = 49.3 Hz, C$_{ipso}$-PPh$_3$), 137.65 (C3), 145.30 (C6). ^{31}P NMR (CDCl$_3$): δ/ppm 41.65 (s, P-PPh$_3$). UV−vis (CHCl$_3$): λ_{max}/nm ($\varepsilon/10^4$ M^{-1} cm^{-1}) 484 (0.7). Anal. Calcd for C$_{29}$H$_{22}$NNiO$_2$PS·$^1/_5$CH$_2$Cl$_2$: C, 63.17; H, 4.07; N, 2.52; S, 5.78. Found: C, 63.00; H, 4.10; N, 2.60; S, 6.00.

Synthesis of Ni(η^5-C$_5$H$_5$)(PPh$_3$)(C≡C{C$_4$H$_2$S}$_2$NO$_2$) (2Ni). Ni(η^5-C$_5$H$_5$)(PPh$_3$)Cl (0.42 g, 1.0 mmol), **2′** (0.26 g, 1.10 mmol), and CuI (0.015 g, 0.08 mmol) were suspended in NEt$_3$/THF 4/1 (30 mL). After the mixture was stirred at room temperature for 16 h, the solvent was removed under vacuum and the resultant solid residue was extracted with dichloromethane and then flash chromatographed on silica gel. Elution with *n*-hexane/Et$_2$O (1/1) gave a red band, from which the desired compound was isolated as a dark red solid in 78% yield (0.48 g). ν(KBr)/cm^{-1}: 1314s and 1517s, 2074m (C≡C). ^{1}H NMR (CDCl$_3$): δ/ppm 5.26 (s, 5H, C$_5$H$_5$), 6.27 (d, 1H, $^3J_{HH}$ = 4.2 Hz, H4), 6.80 (d, 1H, $^3J_{HH}$ = 4.0 Hz, H8), 6.94 (d, 1H, $^3J_{HH}$ = 4.2 Hz, H5), 7.74 (d, 1H, $^3J_{HH}$ = 4.0 Hz, H9), 7.39−7.49 and 7.62−7.72 (m, 15H, H-PPh$_3$). ^{13}C NMR (CDCl$_3$): δ/ppm 92.85 (s, C$_5$H$_5$), 110.79 (C2), 120.98 (C8), 126.26 (C5), 128.33 (t, $^3J_{CP}$ = 10.5 Hz, C$_{meta}$-PPh$_3$), 128.98 (C4), 130.00 (C9), 130.36 (C6), 130.37 (s, C$_{para}$-PPh$_3$), 132.11 (C3), 133.29 (t, $^1J_{CP}$ = 49.0 Hz, C$_{ipso}$-PPh$_3$), 133.75 (t, $^2J_{CP}$ = 11.0 Hz, C$_{ortho}$-PPh$_3$), 134.46 (t, $^2J_{CP}$ = 21.8 Hz, C1), 146.21 (C7), 147.78 (C10). ^{31}P NMR (CDCl$_3$): δ/ppm 41.14 (s, P-PPh$_3$). UV−vis (CHCl$_3$): λ_{max}/nm ($\varepsilon/10^4$ M^{-1} cm^{-1}) 506 (2.3). Anal. Calcd for C$_{33}$H$_{24}$NNiO$_2$PS$_2$·$^1/_4$CH$_2$Cl$_2$: C, 62.25; H, 3.85; N, 2.18; S, 10.00. Found: C, 62.10; H, 3.90; N, 2.20; S, 10.00.

Electrochemical Studies. Electrochemical measurements were performed on an EG&G Princeton Applied Research potentiostat/galvanostat Model 273A equipped with Electrochemical PowerSuite v2.51 software for electrochemical analysis, in anhydrous dichloromethane or acetonitrile with tetrabutylammonium hexafluorophosphate (0.1 M) as supporting electrolyte. The electrochemical cell was a homemade three-electrode configuration cell with a platinum-disk

working electrode (1.0 mm) probed by a Luggin capillary connected to a silver-wire pseudoreference electrode and a platinum-wire auxiliary electrode. All of the experiments were performed under a nitrogen atmosphere at room temperature and in some special cases also at −20 °C. All of the potentials reported were measured against the ferrocene/ferrocenium redox couple as internal standard and normally quoted relative to SCE (using the ferrocenium/ferrocene redox couple $E_{1/2}$ = 0.46 or 0.40 V versus SCE for dichloromethane or acetonitrile, respectively[66]). The electrochemical grade electrolyte was purchased from Aldrich Chemical Co. and dried under vacuum at 110 °C for 24 h. Reagent grade solvents were dried, purified by standard procedure,s[61] and distilled under a nitrogen atmosphere before use.

HRS Measurements of the First Hyperpolarizabilities. β measurements were carried out using the harmonic light scattering technique (also named hyper-Rayleigh) in chloroform solutions. The 10^{-3}–10^{-5} M solutions of the complexes were placed into a 4 cm long fluorimetric cell, after being carefully filtered through a 0.2 μm filter in order to eliminate the white light noise resulting from microburning of any the remaining dust particles by the incoming laser beam. The measurements were performed at a fundamental wavelength of 1500 nm as described in ref 67, using a Q-switched Nd:YAG laser operating in the 10 Hz repetition range. Fluorescence checks were made by replacement of the interference filter at the entrance of the photomultiplier tube using filters with the transmittances at 650, 700, and 800 nm. Disperse Red 1 (DR1) was used as an external standard dissolved in chloroform. The reference hyperpolarizability β of DR1 in CHCl$_3$ was measured by comparison of the slopes of I_{2w} vs concentration plot of the standard in CH$_2$Cl$_2$ and CHCl$_3$. Using the hyperpolarizability of DR1 in dichloromethane ($\beta_{DR1}(CH_2Cl_2)$ = 70 × 10^{-30} esu[68]) the hyperpolarizability of DR1 in CHCl$_3$ was estimated to be 80 × 10^{-30} esu, which is very close to the published value of 74 × 10^{-30} esu.[67] Assuming that the scattering contribution from the solvent is negligibly small, this external reference method is used to calculate the β values of complexes according to eq 1, where s is the slope of the appropriate I_{2w} vs concentration plot and β_{ref} is the orientational average of the first hyperpolarizability of the reference sample.

$$\beta = \sqrt{\frac{s_{sample}}{s_{reference}}}\,\beta_{reference} \tag{1}$$

DFT Calculations. All calculations were performed at the DFT level using the Gaussian 09 package.[69] The hybrid functional B3LYP[70,71] (Becke's three-parameter functional with Lee–Yang–Parr exchange correlations) were used for the calculations. As a compromise between accuracy and computational effort we have adopted the 6-31G* basis set (for geometry optimizations) and the 6-31+G* basis set (for the calculation of hyperpolarizabilities) for C, H, N, O, and H and the LANL2DZ effective core potential basis set for S, P, Fe, Ru, and Ni.[72,73] In the case of the hyperpolarizability calculations the LANL2DZ basis set was also augmented with a polarization function (exponents of 0.496 and 0.364) and a diffuse function (exponents of 0.0347 and 0.0298) for elements S and P, respectively.[74−76] Geometry optimizations were performed without any symmetry constraints. In all cases, the Hessian was computed to confirm the stationary points of the potential energy surfaces (PES) as true minima. The static first hyperpolarizability, β_{tot}, for all compounds was calculated by means of the analytic gradient methodology adopted in the Gaussian 09 program package by using the equation

$$\beta_{tot} = \sqrt{\beta_x^2 + \beta_y^2 + \beta_z^2} \tag{2}$$

upon calculating the individual static components

$$\beta_i = \beta_{iii} + \frac{1}{3}\sum_{i \neq j}(\beta_{ijj} + \beta_{jij} + \beta_{jji}) \tag{3}$$

Time-dependent density functional theory (TDDFT)[77,78] was used to compute the electronic spectra of the studied molecules, applying the same theory level and basis sets used for the calculation of the hyperpolarizabilities. The first 24 lower excitation energies were computed, and the simulated absorption bands were obtained by convolution of Gaussian functions centered at the calculated excitation energies using the GaussSum[79] (version 2.2.4) software. The Chemcraft[80] program (version 1.6) was used for the visualization of the computed results, including the representation of the geometries and the orbitals.

■ ASSOCIATED CONTENT

Ⓢ Supporting Information

Text, figures, and tables, giving the justification for the use of the simplifications in DFT calculations, TDDFT calculated absorption spectrum for **2a′Ru**, optimized geometries and β tensors of all computed structures, cyclic voltammetry plots, and selected NMR spectra. This material is available free of charge via the Internet at http://pubs.acs.org.

■ AUTHOR INFORMATION

Corresponding Author
*P.J.M.: e-mail, pjgm@uevora.pt; tel, +351 266745318; fax, +351 26645303.

Notes

The authors declare no competing financial interest.

■ ACKNOWLEDGMENTS

■ REFERENCES

(1) Nalwa, H. S. *Appl. Organomet. Chem.* **1991**, *5*, 349−377.
(2) Long, N. J. *Angew. Chem., Int. Ed. Engl.* **1995**, *34*, 21−38.
(3) Verbiest, T.; Houbrechts, S.; Kauranen, M.; Clays, K.; Persoons, A. *J. Mater. Chem.* **1997**, *7*, 2175−2189.
(4) Whittall, I. R.; McDonagh, A. M.; Humphrey, M. G.; Samoc, M. In *Organometallic Complexes in Nonlinear Optics I: Second-Order Nonlinearities*; Stone, F. G. A., Robert, W., Eds.; Academic Press: New York, 1998; Advances in Organometallic Chemistry *42*, pp 291−362.
(5) Di Bella, S. *Chem. Soc. Rev.* **2001**, *30*, 355−366.
(6) Goovaerts, E.; Wenseleers, W. E.; Garcia, M. H.; Cross, G. H. Design and characterization of organic and organometallic molecules for second order nonlinear optics. In *Handbook of Advanced Electronic and Photonic Materials and Devices*; Nalwa, H. S., Ed.; Academic Press: Burlington, 2001; Chapter 3, pp 127−191.
(7) Powell, C. E.; Humphrey, M. G. *Coord. Chem. Rev.* **2004**, *248*, 725−756.
(8) Cariati, E.; Pizzotti, M.; Roberto, D.; Tessore, F.; Ugo, R. *Coord. Chem. Rev.* **2006**, *250*, 1210−1233.
(9) Bozec, H.; Guerchais, V. *Molecular Organometallic Materials for Optics*; Springer-Verlag: Berlin and Heidelberg, Germany, 2010; p 230.
(10) Morrall, J. P.; Dalton, G. T.; Humphrey, M. G.; Samoc, M. In *Organotransition Metal Complexes for Nonlinear Optics*; West, R., Hill, A., Fink, M. J., Eds.; Academic Press: New York, 2007; Advances in Organometallic Chemistry *55*, pp 61−136.
(11) Heck, J.; Dede, M. Ferrocene-Based Electro-Optical Materials. In *Ferrocenes*; Wiley: Chichester, U.K., 2008; pp 319−392.
(12) Green, K. A.; Cifuentes, M. P.; Samoc, M.; Humphrey, M. G. *Coord. Chem. Rev.* **2011**, *255*, 2025−2038.
(13) Babgi, B.; Rigamonti, L.; Cifuentes, M. P.; Corkery, T. C.; Randles, M. D.; Schwich, T.; Petrie, S.; Stranger, R.; Teshome, A.; Asselberghs, I.; Clays, K.; Samoc, M.; Humphrey, M. G. *J. Am. Chem. Soc.* **2009**, *131*, 10293−10307.
(14) Garcia, M. H.; Florindo, P.; Piedade, M. F. M.; Duarte, M. T.; Robalo, M. P.; Goovaerts, E.; Wenseleers, W. *J. Organomet. Chem.* **2009**, *694*, 433−445.

(15) Garcia, M. H.; Mendes, P. J.; Robalo, M. P.; Duarte, M. T.; Lopes, N. *J. Organomet. Chem.* **2009**, *694*, 2888−2897.

(16) Garcia, M. H.; Mendes, P. J.; Robalo, M. P.; Dias, A. R.; Campo, J.; Wenseleers, W.; Goovaerts, E. *J. Organomet. Chem.* **2007**, *692*, 3027−3041.

(17) Garcia, M. H.; Robalo, M. P.; Dias, A. R.; Piedade, M. F. M.; Galvão, A.; Wenseleers, W.; Goovaerts, E. *J. Organomet. Chem.* **2001**, *619*, 252−264.

(18) Robalo, M. P.; Teixeira, A. P. S.; Garcia, M. H.; Minas da Piedade, M. F.; Duarte, M. T.; Dias, A. R.; Campo, J.; Wenseleers, W.; Goovaerts, E. *Eur. J. Inorg. Chem.* **2006**, *2006*, 2175−2185.

(19) Wenseleers, W.; Goovaerts, E.; Hepp, P.; Garcia, M. H.; Paula Robalo, M.; Dias, A. R.; Piedade, M. F. M.; Duarte, M. T. *Chem. Phys. Lett.* **2003**, *367*, 390−397.

(20) Garcia, M. H.; Robalo, M. P.; Dias, A. R.; Duarte, M. T.; Wenseleers, W.; Aerts, G.; Goovaerts, E.; Cifuentes, M. P.; Hurst, S.; Humphrey, M. G.; Samoc, M.; Luther-Davies, B. *Organometallics* **2002**, *21*, 2107−2118.

(21) Wenseleers, W.; W. Gerbrandij, A.; Goovaerts, E.; Helena Garcia, M.; Paula Robalo, M.; J. Mendes, P.; C. Rodrigues, J.; R. Dias, A. *J. Mater. Chem.* **1998**, *8*, 925−930.

(22) Wu, I.-Y.; Lin, J. T.; Luo, J.; Li, C.-S.; Tsai, C.; Wen, Y. S.; Hsu, C.-C.; Yeh, F.-F.; Liou, S. *Organometallics* **1998**, *17*, 2188−2198.

(23) Mendes, P. J.; Carvalho, A. J. P.; Ramalho, J. P. P. *J. Mol. Struct. (THEOCHEM)* **2009**, *900*, 110−117.

(24) Whittall, I. R.; Humphrey, M. G.; Hockless, D. C. R.; Skelton, B. W.; White, A. H. *Organometallics* **1995**, *14*, 3970−3979.

(25) Whittall, I. R.; Cifuentes, M. P.; Humphrey, M. G.; Luther-Davies, B.; Samoc, M.; Houbrechts, S.; Persoons, A.; Heath, G. A.; Hockless, D. C. R. *J. Organomet. Chem.* **1997**, *549*, 127−137.

(26) Branger, C.; Lequan, M.; Lequan, R. M.; Barzoukas, M.; Fort, A. *J. Mater. Chem.* **1996**, *6*, 555−558.

(27) Chou, S.-S. P.; Sun, D.-J.; Lin, H.-C.; Yang, P.-K. *J. Chem. Soc., Chem. Commun.* **1996**, *0*, 1045−1046.

(28) Rao, V. P.; Jen, A. K. Y.; Wong, K. Y.; Drost, K. J. *J. Chem. Soc., Chem. Commun.* **1993**, *0*, 1118−1120.

(29) Oudar, J. L.; Chemla, D. S. *J. Chem. Phys.* **1977**, *66*, 2664−2668.

(30) Zhang, T.-G.; Zhao, Y.; Asselberghs, I.; Persoons, A.; Clays, K.; Therien, M. J. *J. Am. Chem. Soc.* **2005**, *127*, 9710−9720.

(31) Whittall, I. R.; Humphrey, M. G.; Persoons, A.; Houbrechts, S. *Organometallics* **1996**, *15*, 1935−1941.

(32) Powell, C. E.; Cifuentes, M. P.; McDonagh, A. M.; Hurst, S. K.; Lucas, N. T.; Delfs, C. D.; Stranger, R.; Humphrey, M. G.; Houbrechts, S.; Asselberghs, I.; Persoons, A.; Hockless, D. C. R. *Inorg. Chim. Acta* **2003**, *352*, 9−18.

(33) Whittall, I. R.; Cifuentes, M. P.; Humphrey, M. G.; Luther-Davies, B.; Samoc, M.; Houbrechts, S.; Persoons, A.; Heath, G. A.; Bogsányi, D. *Organometallics* **1997**, *16*, 2631−2637.

(34) Xia, A.; Selegue, J. P. *Inorg. Chim. Acta* **2002**, *334*, 219−224.

(35) McGrady, J. E.; Lovell, T.; Stranger, R.; Humphrey, M. G. *Organometallics* **1997**, *16*, 4004−4011.

(36) Whittall, I. R.; Humphrey, M. G.; Hockless, D. C. R. *Aust. J. Chem.* **1998**, *51*, 219−228.

(37) Pilar Gamasa, M.; Gimeno, J.; Lastra, E.; Lanfranchi, M.; Tiripicchio, A. *J. Organomet. Chem.* **1991**, *405*, 333−345.

(38) H. Naulty, R.; P. Cifuentes, M.; G. Humphrey, M.; Houbrechts, S.; Boutton, C.; Persoons, A.; A. Heath, G.; C. R. Hockless, D.; Luther-Davies, B.; Samoc, M. *J. Chem. Soc., Dalton Trans.* **1997**, 4167−4174.

(39) Whittall, I. R.; Humphrey, M. G.; Houbrechts, S.; Maes, J.; Persoons, A.; Schmid, S.; Hockless, D. C. R. *J. Organomet. Chem.* **1997**, *544*, 277−283.

(40) Mendes, P. J.; Silva, T. J. L.; Carvalho, A. J. P.; Ramalho, J. P. P. *J. Mol. Struct. (THEOCHEM)* **2010**, *946*, 33−42.

(41) Marder, S. R.; Gorman, C. B.; Tiemann, B. G.; Perry, J. W.; Bourhill, G.; Mansour, K. *Science* **1993**, *261*, 186−189.

(42) Janowska, I.; Zakrzewski, J.; Nakatani, K.; Palusiak, M.; Walak, M.; Scholl, H. *J. Organomet. Chem.* **2006**, *691*, 323−330.

(43) Liu, C.-G.; Qiu, Y.-Q.; Sun, S.-L.; Li, N.; Yang, G.-C.; Su, Z.-M. *Chem. Phys. Lett.* **2007**, *443*, 163−168.

(44) Olivier, C.; Kim, B.; Touchard, D.; Rigaut, S. *Organometallics* **2008**, *27*, 509−518.

(45) Olivier, C.; Costuas, K.; Choua, S.; Maurel, V.; Turek, P.; Saillard, J.-Y.; Touchard, D.; Rigaut, S. *J. Am. Chem. Soc.* **2010**, *132*, 5638−5651.

(46) Armitt, D. J.; Bruce, M. I.; Gaudio, M.; Zaitseva, N. N.; Skelton, B. W.; White, A. H.; Le Guennic, B.; Halet, J.-F.; Fox, M. A.; Roberts, R. L.; Hartl, F.; Low, P. J. *Dalton Trans.* **2008**, 6763−6775.

(47) Powell, C. E.; Cifuentes, M. P.; Morrall, J. P.; Stranger, R.; Humphrey, M. G.; Samoc, M.; Luther-Davies, B.; Heath, G. A. *J. Am. Chem. Soc.* **2002**, *125*, 602−610.

(48) Wuttke, E.; Pevny, F.; Hervault, Y.-M.; Norel, L.; Drescher, M.; Winter, R. F.; Rigaut, S. *Inorg. Chem.* **2012**, *51*, 1902−1915.

(49) Costuas, K.; Rigaut, S. *Dalton Trans.* **2011**, *40*, 5643−5658.

(50) Heck, J.; Dabek, S.; Meyer-Friedrichsen, T.; Wong, H. *Coord. Chem. Rev.* **1999**, *190−192*, 1217−1254.

(51) Loukova, G. V. *Chem. Phys. Lett.* **2002**, *353*, 244−252.

(52) Loukova, G. V.; Strelets, V. V. *J. Organomet. Chem.* **2000**, *606*, 203−206.

(53) Campo, J.; Wenseleers, W.; Goovaerts, E.; Szablewski, M.; Cross, G. H. *J. Phys. Chem. C* **2007**, *112*, 287−296.

(54) Campo, J.; Wenseleers, W.; Hales, J. M.; Makarov, N. S.; Perry, J. W. *J. Phys. Chem. Lett.* **2012**, *3*, 2248−2252.

(55) Mang, C.; Wu, K.; Zhang, M.; Hong, T.; Wei, Y. *J. Mol. Struct. (THEOCHEM)* **2004**, *674*, 77−82.

(56) Curreli, S.; Deplano, P.; Faulmann, C.; Ienco, A.; Mealli, C.; Mercuri, M. L.; Pilia, L.; Pintus, G.; Serpe, A.; Trogu, E. F. *Inorg. Chem.* **2004**, *43*, 5069−5079.

(57) Li, Q.; Sa, R.; Liu, C.; Wu, K. *J. Phys. Chem. A* **2007**, *111*, 7925−7932.

(58) Mang, C.; Wu, K. *Int. J. Quantum Chem.* **2006**, *106*, 2529−2535.

(59) Cardoso, C.; Abreu, P. E.; Nogueira, F. *J. Chem. Theory Comput.* **2009**, *5*, 850−858.

(60) Bruschi, M.; Fantucci, P.; Pizzotti, M. *J. Phys. Chem. A* **2005**, *109*, 9637−9645.

(61) Armarego, W. L. F.; Chai, C. L. L. *Purification of Laboratory Chemicals*, 5th ed.; Elsevier: Amsterdam, 2003.

(62) Ashby, G. S.; Bruce, M. I.; Tomkins, I. B.; Wallis, R. C. *Aust. J. Chem.* **1979**, *32*, 1003−1016.

(63) Barnett, K. W. *J. Chem. Educ.* **1974**, *51*, 422.

(64) Bäuerle, P.; Würthner, F.; Götz, G.; Effenberger, F. *Synthesis* **1993**, *1993* (1099), 1103.

(65) Laszlo, P.; Cornelis, A. *Aldrichim. Acta* **1988**, *21*, 6.

(66) Connelly, N. G.; Geiger, W. E. *Chem. Rev.* **1996**, *96*, 877−910.

(67) Stadler, S.; Dietrich, R.; Bourhill, G.; Bräuchle, C.; Pawlik, A.; Grahn, W. *Chem. Phys. Lett.* **1995**, *247*, 271−276.

(68) Ipaktschi, J.; Mohseni-Ala, J.; Dülmer, A.; Steffens, S.; Wittenburg, C.; Heck, J. *Organometallics* **2004**, *23*, 4902−4909.

(69) Frisch, M. J.; Trucks, G. W.; Schlegel, H. B.; Scuseria, G. E.; Robb, M. A.; Cheeseman, J. R.; Scalmani, G.; Barone, V.; Mennucci, B.; Petersson, G. A.; Nakatsuji, H.; Caricato, M.; Li, X.; Hratchian, H. P.; Izmaylov, A. F.; Bloino, J.; Zheng, G.; Sonnenberg, J. L.; Hada, M.; Ehara, M.; Toyota, K.; Fukuda, R.; Hasegawa, J.; Ishida, M.; Nakajima, T.; Honda, Y.; Kitao, O.; Nakai, H.; Vreven, T.; Montgomery, J. A.; Peralta, J. E.; Ogliaro, F.; Bearpark, M.; Heyd, J. J.; Brothers, E.; Kudin, K. N.; Staroverov, V. N.; Kobayashi, R.; Normand, J.; Raghavachari, K.; Rendell, A.; Burant, J. C.; Iyengar, S. S.; Tomasi, J.; Cossi, M.; Rega, N.; Millam, J. M.; Klene, M.; Knox, J. E.; Cross, J. B.; Bakken, V.; Adamo, C.; Jaramillo, J.; Gomperts, R.; Stratmann, R. E.; Yazyev, O.; Austin, A. J.; Cammi, R.; Pomelli, C.; Ochterski, J. W.; Martin, R. L.; Morokuma, K.; Zakrzewski, V. G.; Voth, G. A.; Salvador, P.; Dannenberg, J. J.; Dapprich, S.; Daniels, A. D.; Farkas; Foresman, J. B.; Ortiz, J. V.; Cioslowski, J.; Fox, D. J. *Gaussian 09, Revision A.01*; Gaussian, Inc., Wallingford, CT, 2009.

(70) Becke, A. D. *J. Chem. Phys.* **1993**, *98*, 5648−5652.

(71) Lee, C.; Yang, W.; Parr, R. G. *Phys. Rev. B* **1988**, *37*, 785−789.

(72) Hay, P. J.; Wadt, W. R. *J. Chem. Phys.* **1985**, *82*, 270−283.

(73) Hay, P. J.; Wadt, W. R. *J. Chem. Phys.* **1985**, *82*, 299−310.

(74) Check, C. E.; Faust, T. O.; Bailey, J. M.; Wright, B. J.; Gilbert, T. M.; Sunderlin, L. S. *J. Phys. Chem. A* **2001**, *105*, 8111−8116.

(75) Feller, D. *J. Comput. Chem.* **1996**, *17*, 1571−1586.

(76) Schuchardt, K. L.; Didier, B. T.; Elsethagen, T.; Sun, L.; Gurumoorthi, V.; Chase, J.; Li, J.; Windus, T. L. *J. Chem. Inf. Model.* **2007**, *47*, 1045−1052.

(77) Nalewajski, R. Density Functional Theory. In *Perspectives in Electronic Structure Theory*; Springer: Berlin and Heidelberg, Germany, 2011; pp 255−368.

(78) Casida, M. E.; Jamorski, C.; Casida, K. C.; Salahub, D. R. *J. Chem. Phys.* **1998**, *108*, 4439−4449.

(79) O'Boyle, N. M.; Tenderholt, A. L.; Langner, K. M. *J. Comput. Chem.* **2008**, *29*, 839−845.

(80) Zhurko, G. A. Z. D. A. *ChemCraft: Tool for treatment of chemical data, build 342*; http://www.chemcraftprog.com.